

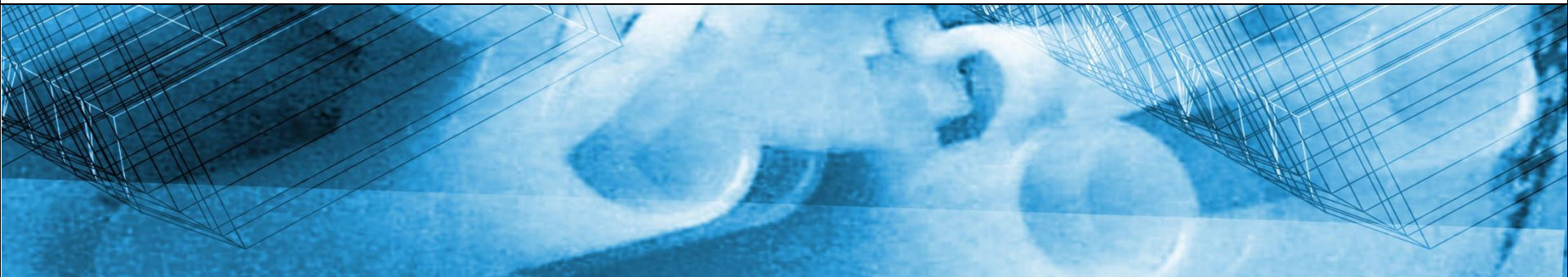
MAGNETIC RESONANCE IMAGING GROUP

Prof. Elfar Adalsteinsson

<http://www.rle.mit.edu/mri>

- I am a grad student at the MRI group, working with Prof. Elfar Adalsteinsson
- We are affiliated with:   
- I have been working on medical image reconstruction using probabilistic analysis & optimization methods.

1. Joint Bayesian compressed sensing for multi-contrast reconstruction:
reconstruct images with different contrasts from undersampled data
2. Quantitative Susceptibility Mapping with magnitude prior:
estimate tissue iron concentration from MRI signal phase
3. Estimating brain iron concentration in normal aging using L1-QSM:
compare brain iron concentration in young & elderly subjects



Joint Bayesian Compressed Sensing for Multi-contrast Reconstruction

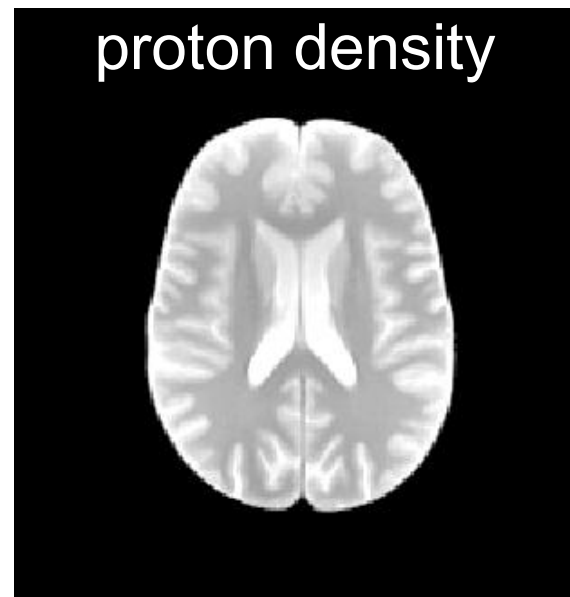
Berkin Bilgic¹, Vivek K. Goyal¹, Elfar Adalsteinsson^{1,2}

¹EECS, MIT, Cambridge, MA, United States

²Harvard-MIT Division of Health Sciences and Technology, Cambridge, MA, United States

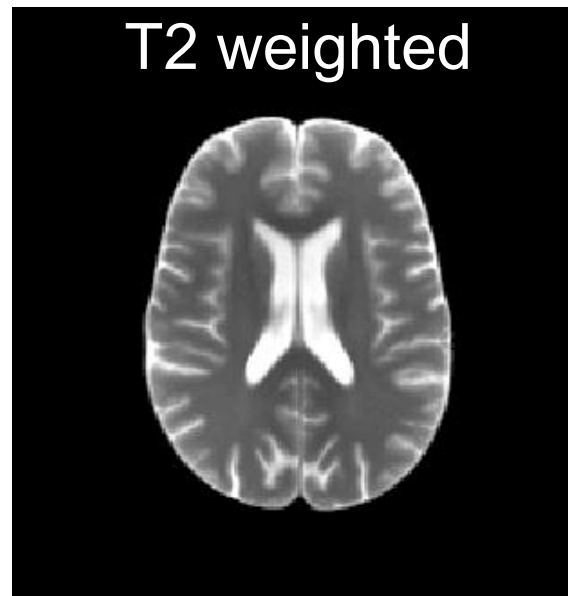
Multi-contrast data acquisition

- ❖ In clinical MRI, it is common to image the same region of interest under multiple contrast settings
- ❖ This aims to increase the diagnostic power of MRI as tissues exhibit different characteristics under different contrasts
- ❖ For instance, SRI24 atlas¹ contains such multi-contrast data,



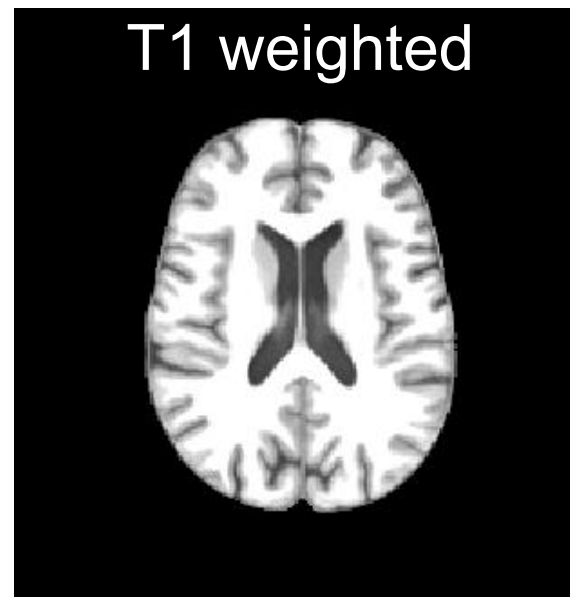
Multi-contrast data acquisition

- ❖ In clinical MRI, it is common to image the same region of interest under multiple contrast settings
- ❖ This aims to increase the diagnostic power of MRI as tissues exhibit different characteristics under different contrasts
- ❖ For instance, SRI24 atlas¹ contains such multi-contrast data,



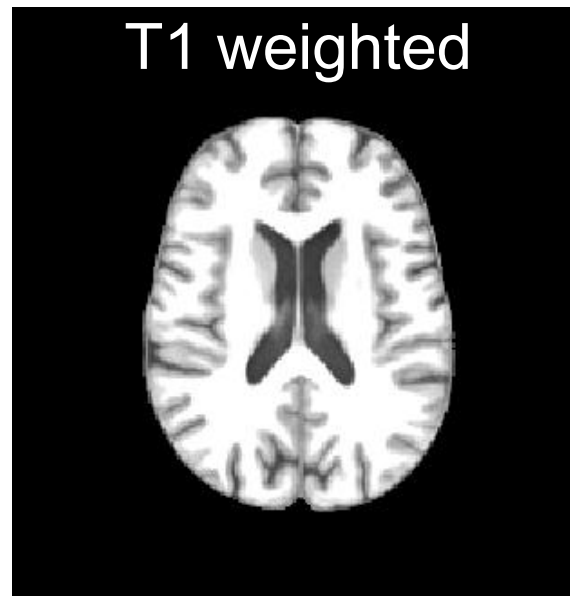
Multi-contrast data acquisition

- ❖ In clinical MRI, it is common to image the same region of interest under multiple contrast settings
- ❖ This aims to increase the diagnostic power of MRI as tissues exhibit different characteristics under different contrasts
- ❖ For instance, SRI24 atlas¹ contains such multi-contrast data,



Multi-contrast data acquisition

- ❖ In clinical MRI, it is common to image the same region of interest under multiple contrast settings
- ❖ This aims to increase the diagnostic power of MRI as tissues exhibit different characteristics under different contrasts
- ❖ For instance, SRI24 atlas¹ contains such multi-contrast data,



Undersampling the k -space

- ❖ To reduce data acquisition time, it is possible to collect a subset of k -space frequencies below the Nyquist rate due to

$$\mathbf{y} = \mathbf{F}_{\Omega} \mathbf{x} + \mathbf{n}$$

$\mathbf{y} \in \mathbb{C}^K$ is the undersampled k -space data,

$\mathbf{F}_{\Omega} \in \mathbb{C}^{K \times M}$ is the undersampled 2D-DFT matrix, with $K < M$

$\mathbf{x} \in \mathbb{R}^M$ is the spatial image and,

$\mathbf{n} \in \mathbb{C}^K$ is the noise in k -space

Undersampling the k -space

- ❖ To reduce data acquisition time, it is possible to collect a subset of k -space frequencies below the Nyquist rate due to

$$\mathbf{y} = \mathbf{F}_{\Omega} \mathbf{x} + \mathbf{n}$$

$\mathbf{y} \in \mathbb{C}^K$ is the undersampled k -space data,

$\mathbf{F}_{\Omega} \in \mathbb{C}^{K \times M}$ is the undersampled 2D - DFT matrix, with $K < M$

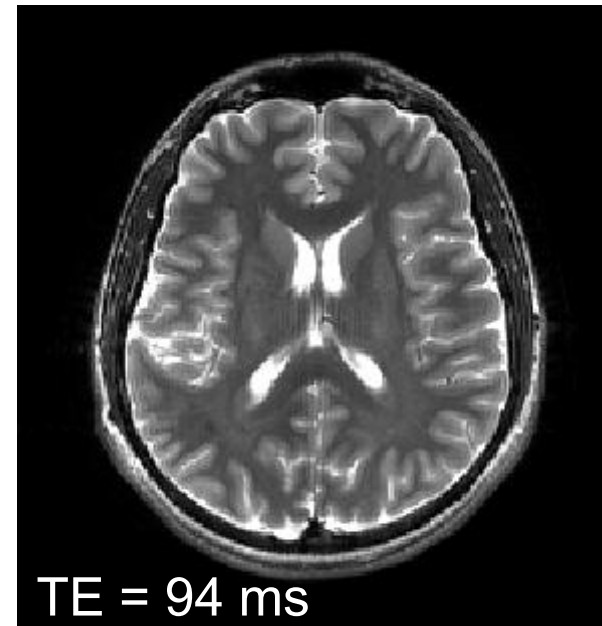
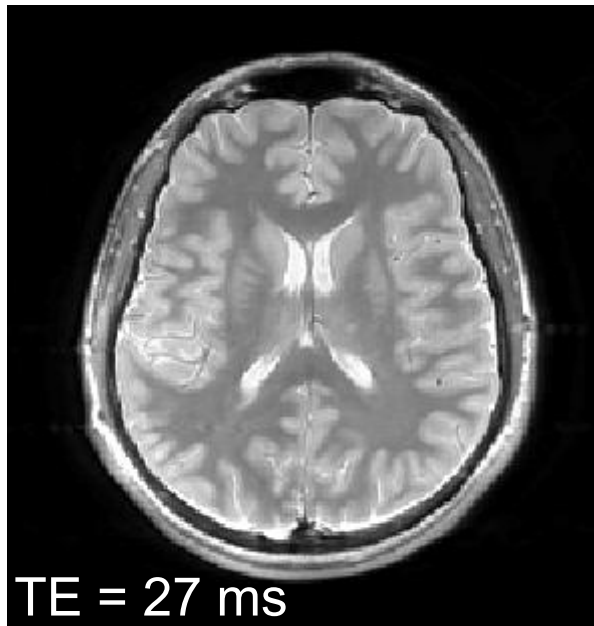
$\mathbf{x} \in \mathbb{R}^M$ is the spatial image and,

$\mathbf{n} \in \mathbb{C}^K$ is the noise in k -space

- ❖ This work aims to reconstruct multi-contrast data from undersampled acquisitions by making use of
 - Bayesian Compressed Sensing theory and,
 - The similarity between the different contrast images.

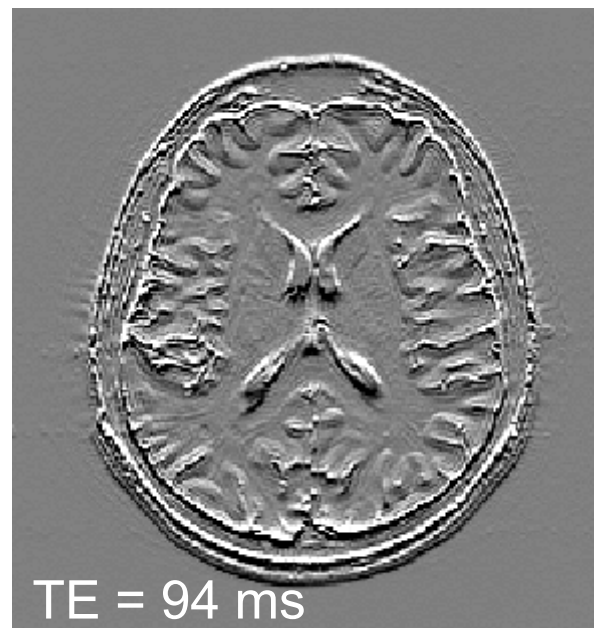
Similarity of multi-contrast images

- ❖ Multi-contrast images possess unique properties, e.g. intensity levels at a given voxel



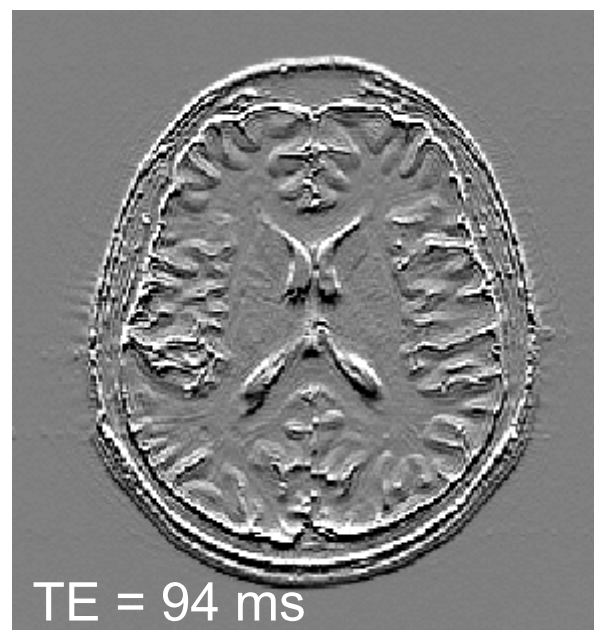
Similarity of multi-contrast images

- ❖ Multi-contrast images possess unique properties, e.g. intensity levels at a given voxel
- ❖ At the same time exhibit common features. We make use of the similarity in sparsity support under gradient transform



Similarity of multi-contrast images

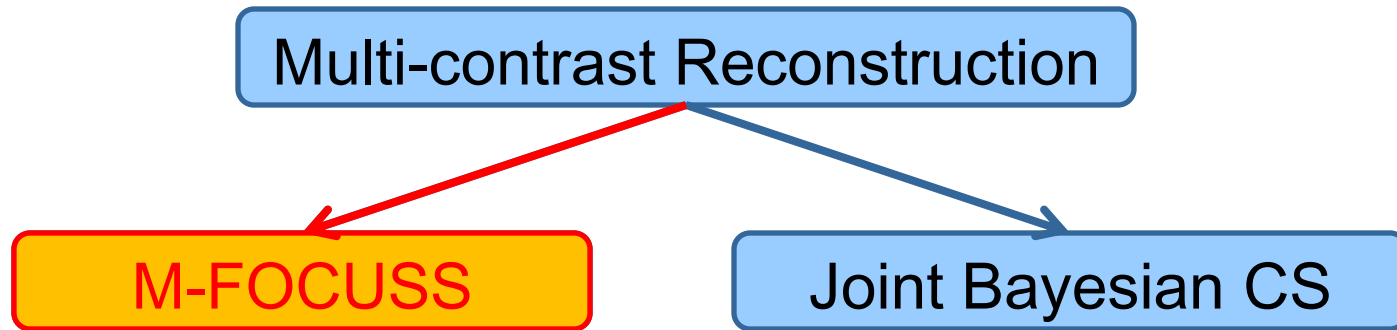
- ❖ Multi-contrast images possess unique properties, e.g. intensity levels at a given voxel
- ❖ At the same time exhibit common features. We make use of the similarity in sparsity support under gradient transform



- Positions of non-zero coefficients are similar, even though there is no perfect overlap

Joint reconstruction algorithms

- ❖ We consider two joint reconstruction algorithms,



- ❖ And first introduce the M-FOCUSS method.

M-FOCUSS algorithm

- ❖ First approach is based on using an existing algorithm, **M-FOCUSS**¹ (**M**ultiple-**FOC**al **U**nderdetermined **S**ystem **S**olver) for joint reconstruction

M-FOCUSS algorithm

- ❖ First approach is based on using an existing algorithm, **M-FOCUSS**¹ (**M**ultiple-**FO**CAl **U**nderdetermined **S**ystem **S**olver) for joint reconstruction
- ❖ M-FOCUSS places an ℓ_1 norm penalty on the gradient coefficients of each image, and an ℓ_2 norm penalty across the multi-contrast images

$$\min_{\mathbf{x}_i} \sum_{i=1}^L \|\mathbf{F}_\Omega \mathbf{x}_i - \mathbf{y}_i\|_2^2 + \lambda \cdot \sum_{j=1}^M \left(\sum_{i=1}^L |\partial \mathbf{x}_{i,j}|^2 \right)^{1/2}$$

M-FOCUSS algorithm

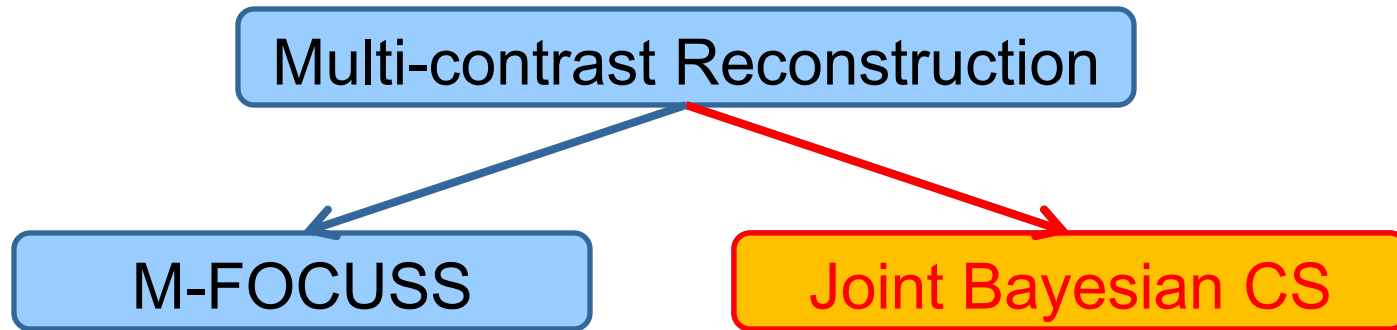
- ❖ First approach is based on using an existing algorithm, **M-FOCUSS**¹ (**M**ultiple-**FO**CAl **U**nderdetermined **S**ystem **S**olver) for joint reconstruction
- ❖ M-FOCUSS places an ℓ_1 norm penalty on the gradient coefficients of each image, and an ℓ_2 norm penalty across the multi-contrast images

$$\min_{\mathbf{x}_i} \sum_{i=1}^L \|\mathbf{F}_{\Omega} \mathbf{x}_i - \mathbf{y}_i\|_2^2 + \lambda \cdot \sum_{j=1}^M \left(\sum_{i=1}^L |\partial \mathbf{x}_{i,j}|^2 \right)^{1/2}$$

- ❖ As proposed, it is constrained to use the same undersampling pattern for each image
- ❖ And makes the strict assumption that the sparsity supports of the images are the same.

Joint reconstruction algorithms

- ❖ We consider two joint reconstruction algorithms,



- ❖ Next, we introduce our joint Bayesian reconstruction method.

Sparse representation and data likelihood

- ❖ To obtain a sparse representation of the images $\{x_i\}_{i=1}^L$ with L different contrasts, we augment the undersampled k -space data $\{y_i\}_{i=1}^L$ as

$$\left(1 - e^{-2\pi j \omega / n}\right) \cdot y_i(\omega, \nu) = \mathbf{F}_{\Omega_i} \delta_i^x \equiv y_i^x$$

$\delta_i^x \in \mathbb{R}^M$ is i^{th} vertical image gradient

$y_i^x \in \mathbb{C}^{K_i}$ is the undersampled k -space data of δ_i^x

Sparse representation and data likelihood

- ❖ To obtain a sparse representation of the images $\{x_i\}_{i=1}^L$ with L different contrasts, we augment the undersampled k -space data $\{y_i\}_{i=1}^L$ as

$$\left(1 - e^{-2\pi j \omega / n}\right) \cdot y_i(\omega, \nu) = \mathbf{F}_{\Omega_i} \delta_i^x \equiv y_i^x$$

$\delta_i^x \in \mathbb{R}^M$ is i^{th} vertical image gradient

$y_i^x \in \mathbb{C}^{K_i}$ is the undersampled k -space data of δ_i^x

- ❖ Modeling the k -space noise to be Gaussian with zero mean and variance σ^2 , the likelihood of observing the data becomes

$$\left. \begin{array}{l} Y_i^x = \left[\mathcal{R}e(y_i^x), \mathcal{I}m(y_i^x) \right]^T \\ \Phi_i = \left[\mathcal{R}e(\mathbf{F}_{\Omega_i}), \mathcal{I}m(\mathbf{F}_{\Omega_i}) \right]^T \end{array} \right\} p(Y_i^x / \delta_i^x, \sigma^2) = (2\pi\sigma^2)^{-K_i} \exp\left(-\|Y_i^x - \Phi_i \delta_i^x\|_2^2 / 2\sigma^2\right)$$

Bayesian analysis for joint inference

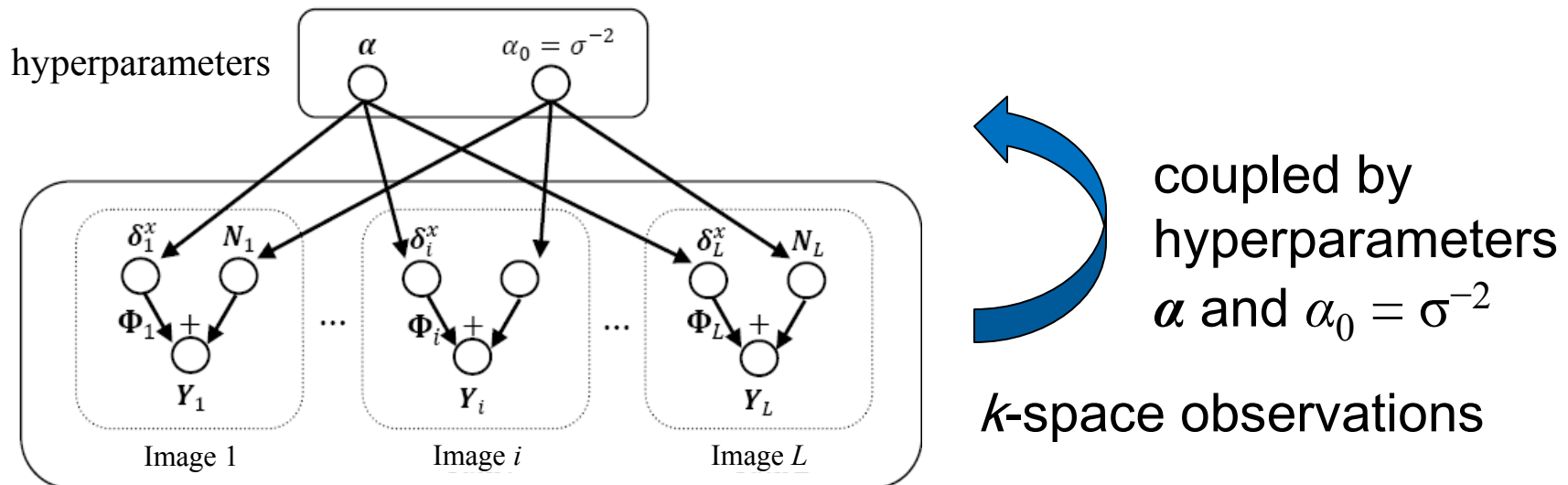
- ❖ Next, we would like to impose a sparsity promoting prior distribution over the image gradients $\{\delta_i^x\}_{i=1}^L$ and $\{\delta_i^y\}_{i=1}^L$,
- ❖ And compute their posterior distribution with the Bayes' rule using this prior, the likelihood term and the observed k -space data $\{\mathbf{Y}_i^x\}_{i=1}^L$ and $\{\mathbf{Y}_i^y\}_{i=1}^L$
- ❖ At the same time, we would like to enable information sharing across the multi-contrast images.

Bayesian analysis for joint inference

- ❖ Next, we would like to impose a sparsity promoting prior distribution over the image gradients $\{\delta_i^x\}_{i=1}^L$ and $\{\delta_i^y\}_{i=1}^L$,
- ❖ And compute their posterior distribution with the Bayes' rule using this prior, the likelihood term and the observed k -space data $\{\mathbf{Y}_i^x\}_{i=1}^L$ and $\{\mathbf{Y}_i^y\}_{i=1}^L$
- ❖ At the same time, we would like to enable information sharing across the multi-contrast images.
- ❖ To this end, we carry out the inference within a hierarchical Bayesian model¹

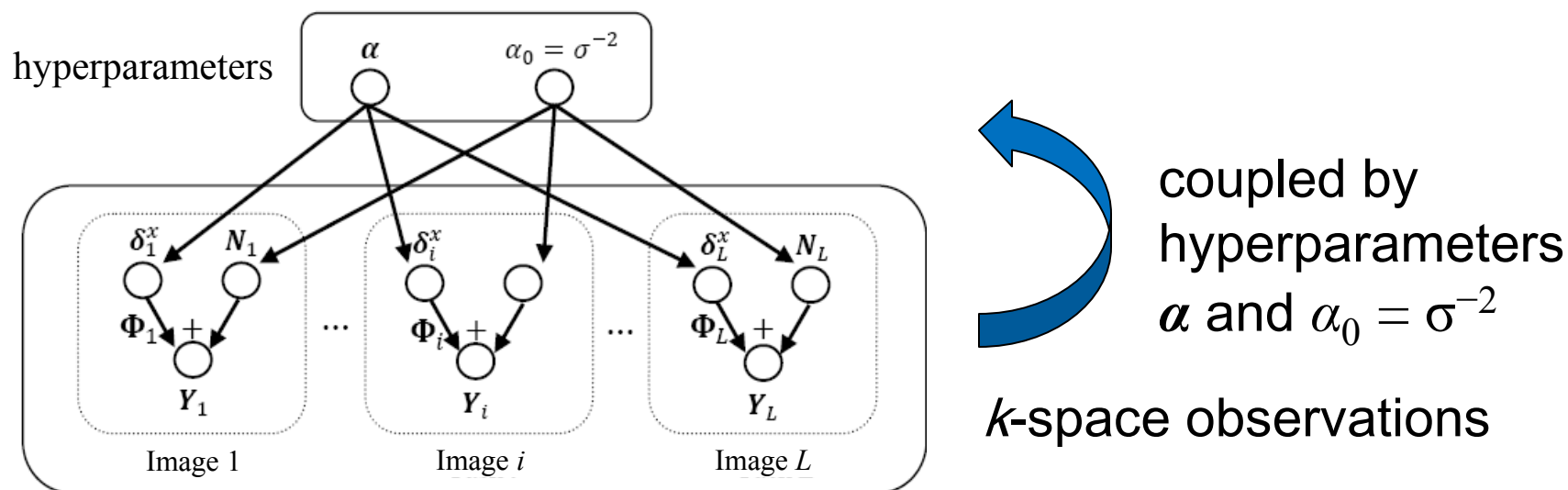
Hierarchical Bayesian Model for joint inference

- ❖ At the bottom layer, we have the undersampled k -space observations, which are jointly parameterized by the hyperparameters on the layer above.



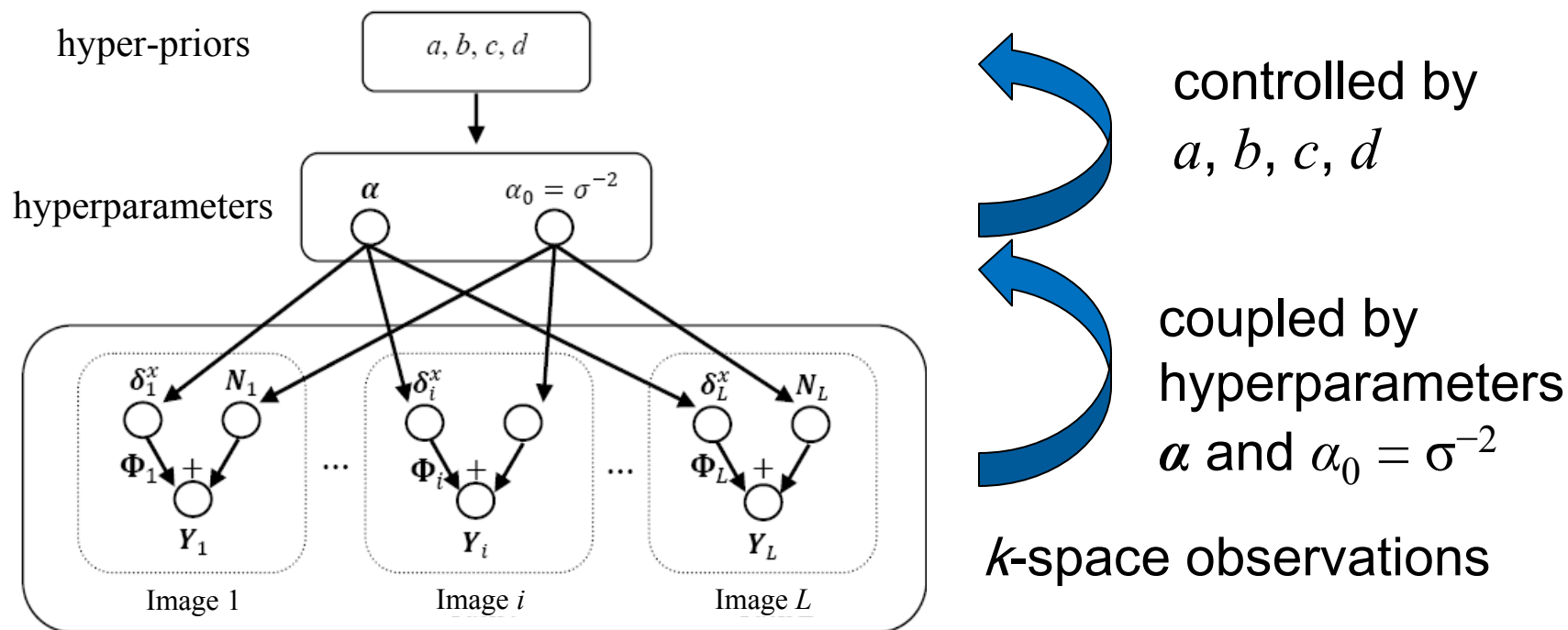
Hierarchical Bayesian Model for joint inference

- ❖ At the bottom layer, we have the undersampled k -space observations, which are jointly parameterized by the hyperparameters on the layer above.
- ❖ We capture the similarity in the gradient domain by defining the hyperparameters α over the L gradient images



Hierarchical Bayesian Model for joint inference

- ❖ At the bottom layer, we have the undersampled k -space observations, which are jointly parameterized by the hyperparameters on the layer above.
- ❖ We capture the similarity in the gradient domain by defining the hyperparameters α over the L gradient images
- ❖ The hyperparameters are in turn controlled by the hyper-priors at the top level.



Prior on the signal coefficients

- ❖ The gradient coefficients are modeled to be drawn from a product of zero mean Gaussians

$$p(\boldsymbol{\delta}_i^x | \boldsymbol{\alpha}) = \prod_{j=1}^M \mathcal{N}(\delta_{i,j}^x | 0, \alpha_j^{-1})$$

and the precisions of the Gaussians are determined by $\boldsymbol{\alpha} \in \mathbb{R}^M$

- ❖ And Gamma priors are placed over the hyperparameters $\boldsymbol{\alpha}$

$$p(\boldsymbol{\alpha} | c, d) = \prod_{j=1}^M \text{Ga}(\alpha_j | c, d) \quad \text{where } \text{Ga}(\alpha_j | c, d) = \frac{d^c}{\Gamma(c)} \alpha_j^{c-1} \exp(-d\alpha_j)$$

Prior on the signal coefficients

- ❖ The gradient coefficients are modeled to be drawn from a product of zero mean Gaussians

$$p(\delta_i^x | \alpha) = \prod_{j=1}^M \mathcal{N}(\delta_{i,j}^x | 0, \alpha_j^{-1})$$

and the precisions of the Gaussians are determined by $\alpha \in \mathbb{R}^M$

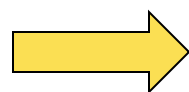
- ❖ And Gamma priors are placed over the hyperparameters α

$$p(\alpha | c, d) = \prod_{j=1}^M \text{Ga}(\alpha_j | c, d) \quad \text{where } \text{Ga}(\alpha_j | c, d) = \frac{d^c}{\Gamma(c)} \alpha_j^{c-1} \exp(-d\alpha_j)$$

- ❖ We can marginalize over the hyperparameters α and obtain the *marginal* prior that enforces sparsity

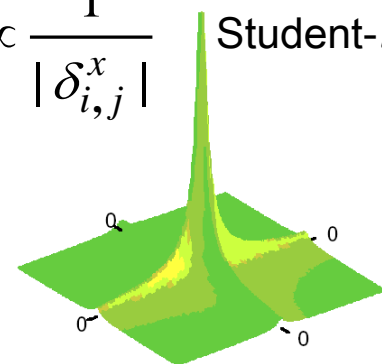
$$p(\delta_{i,j}^x) = \int p(\delta_{i,j}^x / \alpha_j) p(\alpha_j | c, d) d\alpha_j$$

sharp peak at 0



$c, d = 0$

$$p(\delta_{i,j}^x) \propto \frac{1}{|\delta_{i,j}^x|} \quad \text{Student-}t$$



Computing the posterior for the signals

- ❖ Since the data likelihood and the signal prior are both Gaussian, the posterior for the gradient coefficients is also in the same family,

$$p(\boldsymbol{\delta}_i^x | \mathbf{Y}_i^x, \boldsymbol{\alpha}, \alpha_0) = \frac{p(\mathbf{Y}_i^x | \boldsymbol{\delta}_i^x, \alpha_0) p(\boldsymbol{\delta}_i^x | \boldsymbol{\alpha})}{p(\mathbf{Y}_i^x | \boldsymbol{\alpha}, \alpha_0)}$$

Computing the posterior for the signals

- ❖ Since the data likelihood and the signal prior are both Gaussian, the posterior for the gradient coefficients is also in the same family,

$$\text{posterior} \\ p(\delta_i^x | Y_i^x, \alpha, \alpha_0) = \frac{p(Y_i^x | \delta_i^x, \alpha_0) p(\delta_i^x | \alpha)}{p(Y_i^x | \alpha, \alpha_0)}$$

Computing the posterior for the signals

- ❖ Since the data likelihood and the signal prior are both Gaussian, the posterior for the gradient coefficients is also in the same family,

$$\text{posterior } p(\delta_i^x | Y_i^x, \alpha, \alpha_0) = \frac{\text{likelihood } p(Y_i^x | \delta_i^x, \alpha_0) p(\delta_i^x | \alpha)}{p(Y_i^x | \alpha, \alpha_0)}$$

Computing the posterior for the signals

- ❖ Since the data likelihood and the signal prior are both Gaussian, the posterior for the gradient coefficients is also in the same family,

$$\text{posterior } p(\delta_i^x | Y_i^x, \alpha, \alpha_0) = \frac{\text{likelihood } p(Y_i^x | \delta_i^x, \alpha_0) \text{ prior } p(\delta_i^x | \alpha)}{p(Y_i^x | \alpha, \alpha_0)}$$

Computing the posterior for the signals

- ❖ Since the data likelihood and the signal prior are both Gaussian, the posterior for the gradient coefficients is also in the same family,

$$p(\delta_i^x | Y_i^x, \alpha, \alpha_0) = \frac{\overset{\text{Gaussian}}{p(Y_i^x | \delta_i^x, \alpha_0)} \overset{\text{Gaussian}}{p(\delta_i^x | \alpha)}}{p(Y_i^x | \alpha, \alpha_0)}$$

Computing the posterior for the signals

- ❖ Since the data likelihood and the signal prior are both Gaussian, the posterior for the gradient coefficients is also in the same family,

$$\begin{array}{c} \text{also Gaussian} \\ p(\delta_i^x | Y_i^x, \alpha, \alpha_0) \end{array} = \frac{\begin{array}{c} \text{Gaussian} \\ p(Y_i^x | \delta_i^x, \alpha_0) \end{array} \begin{array}{c} \text{Gaussian} \\ p(\delta_i^x | \alpha) \end{array}}{p(Y_i^x | \alpha, \alpha_0)}$$

Computing the posterior for the signals

- ❖ Since the data likelihood and the signal prior are both Gaussian, the posterior for the gradient coefficients is also in the same family,

$$\text{also Gaussian } p(\delta_i^x | Y_i^x, \alpha, \alpha_0) = \frac{\overset{\text{Gaussian}}{p(Y_i^x | \delta_i^x, \alpha_0)} \overset{\text{Gaussian}}{p(\delta_i^x | \alpha)}}{p(Y_i^x | \alpha, \alpha_0)}$$

We only need to estimate the α_i 's

$$\delta_i^x \approx \mathcal{N}(\mu_i, \Sigma_i)$$

$$\mu_i = \alpha_0 \Sigma_i \Phi_i^T Y_i^x$$

$$\Sigma_i = (\alpha_0 \Phi_i^T \Phi_i + \mathbf{A})^{-1}$$

$$\mathbf{A} = \text{diag}(\alpha_1, \alpha_2, \dots, \alpha_M)$$

Maximum Likelihood estimation of hyperparameters

- ❖ We seek point estimates for the hyperparameters α and α_0 in a maximum likelihood framework.

$$\max_{\alpha, \alpha_0} \mathcal{L}(\alpha, \alpha_0) = \max_{\alpha, \alpha_0} \sum_{i=1}^L \log p(\mathbf{Y}_i^x | \alpha, \alpha_0)$$

- ❖ Summation over the L images enables **information sharing** while estimating the hyperparameters.
- ❖ Once the hyperparameters are estimated, the posterior for the gradient coefficients δ_i^x is determined based only on its related k -space data \mathbf{Y}_i^x due to,

$$\boldsymbol{\mu}_i = \alpha_0 \boldsymbol{\Sigma}_i \boldsymbol{\Phi}_i^T \mathbf{Y}_i^x$$

Reconstructing the images from their gradients

❖ After estimating the vertical and horizontal gradients

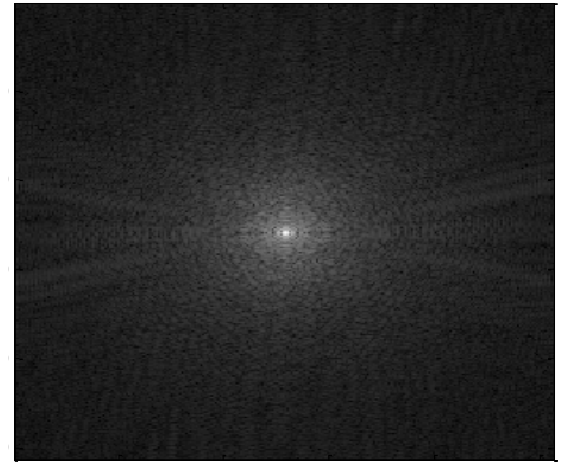
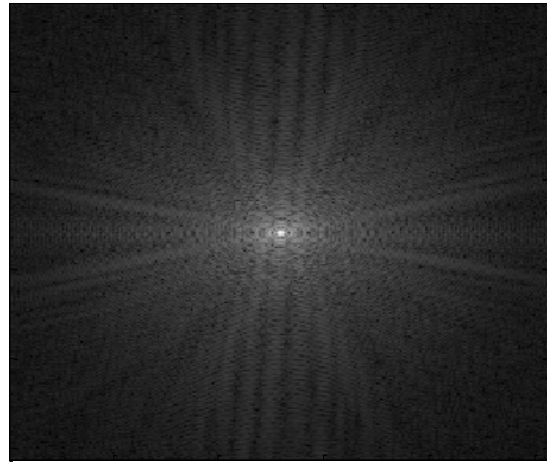
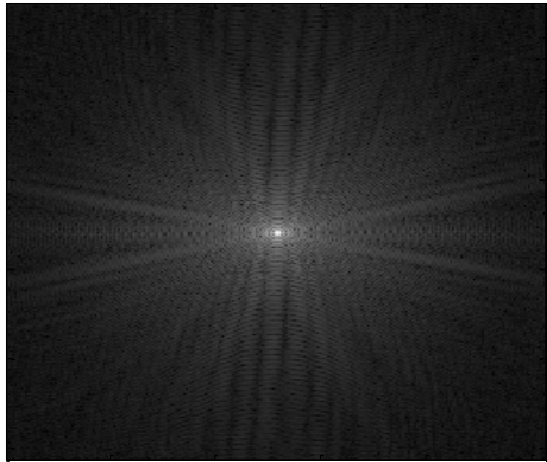
$\{\delta_i^x\}_{i=1}^L$ and $\{\delta_i^y\}_{i=1}^L$, we seek the images $\{\mathbf{x}_i\}_{i=1}^L$ consistent with these and the k -space data $\{\mathbf{y}_i\}_{i=1}^L$ in a Least Squares setting,

$$\hat{\mathbf{x}}_i = \underset{\mathbf{x}_i}{\operatorname{argmin}} \left\| \partial_x \mathbf{x}_i - \delta_i^x \right\|_2^2 + \left\| \partial_y \mathbf{x}_i - \delta_i^y \right\|_2^2 + \lambda \left\| \mathbf{F}_{\Omega_i} \mathbf{x}_i - \mathbf{y}_i \right\|_2^2$$

for $i = 1, \dots, L$

where ∂_x and ∂_y are vertical and horizontal gradient operators

SRI24 Atlas



k -space, 100 % of Nyquist rate



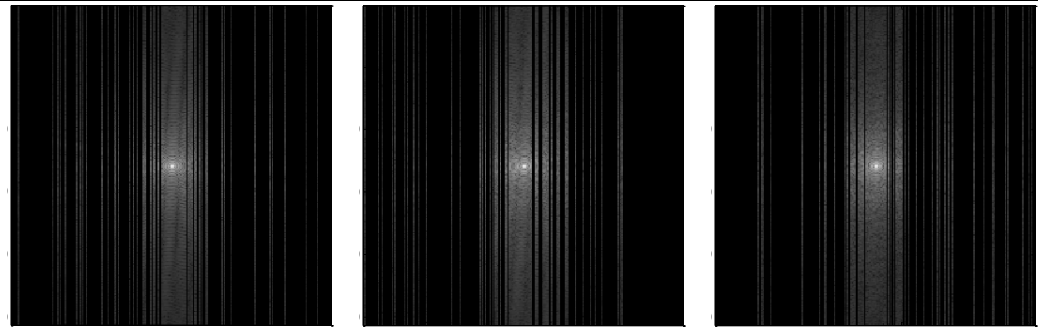
Inverse FFT Error: 0 % RMSE



0.7

0

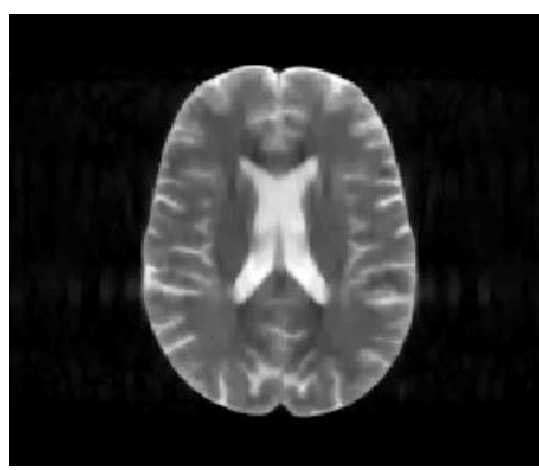
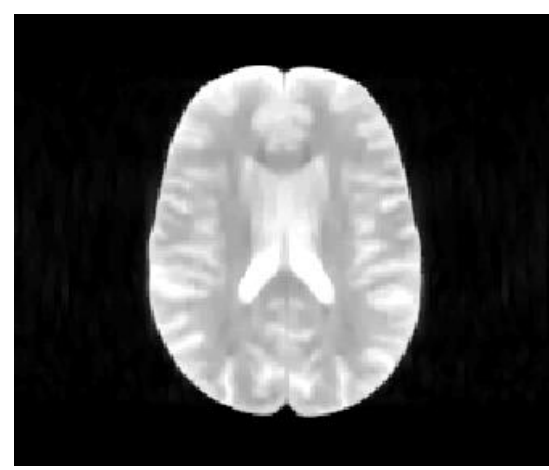
Lustig *et al.*  9.4 %



k-space, 25 % of Nyquist rate

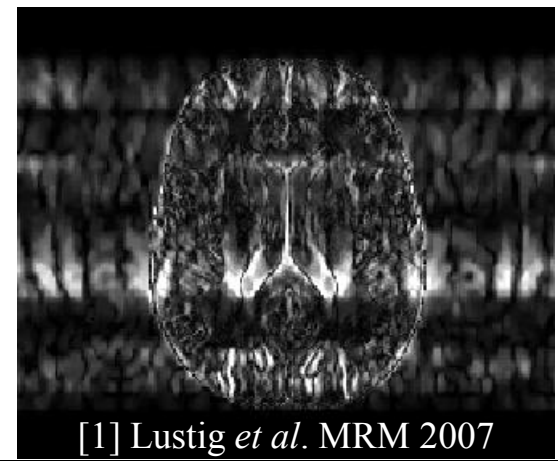
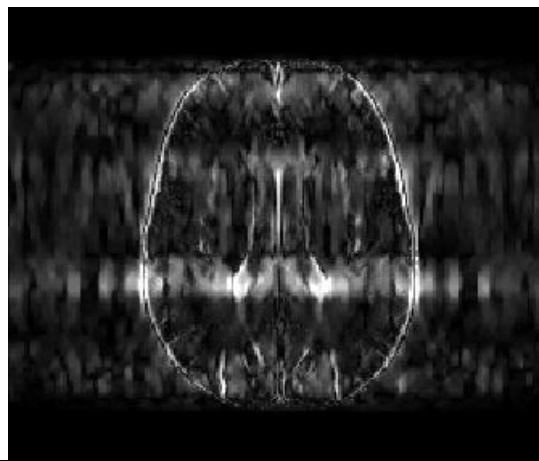
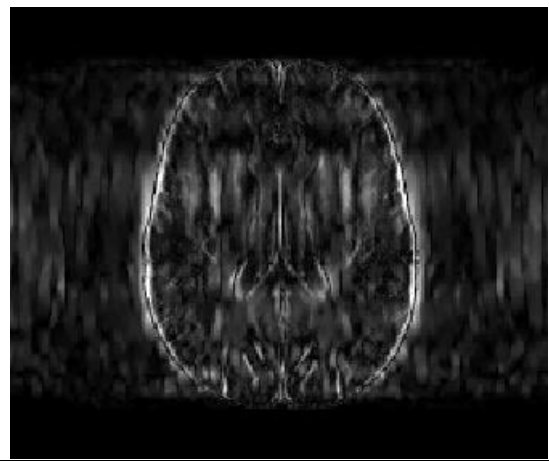


Lustig *et al.*¹ Error: 9.4 % RMSE



0.7

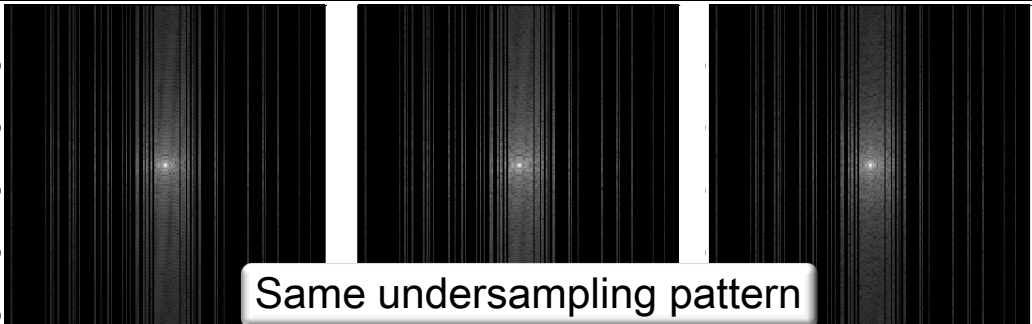
0



0.15

0

[1] Lustig *et al.* MRM 2007

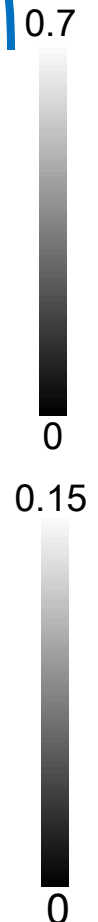
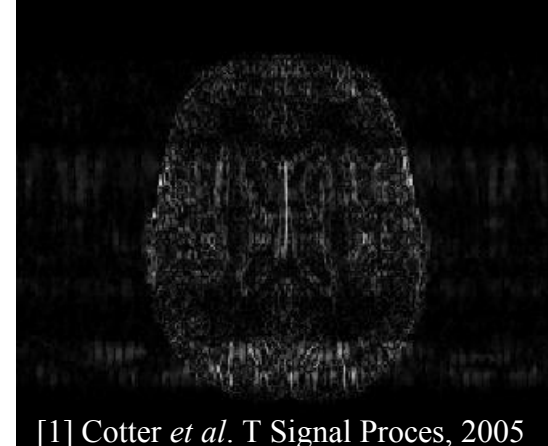
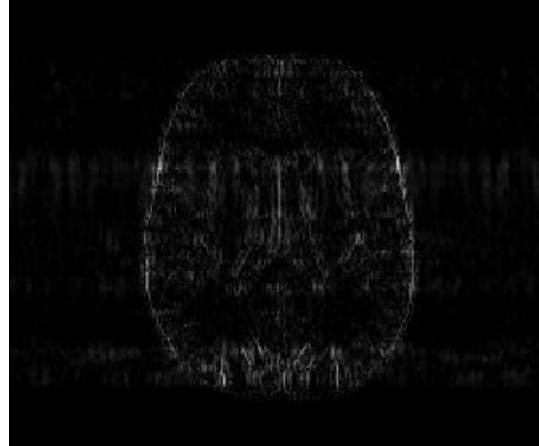
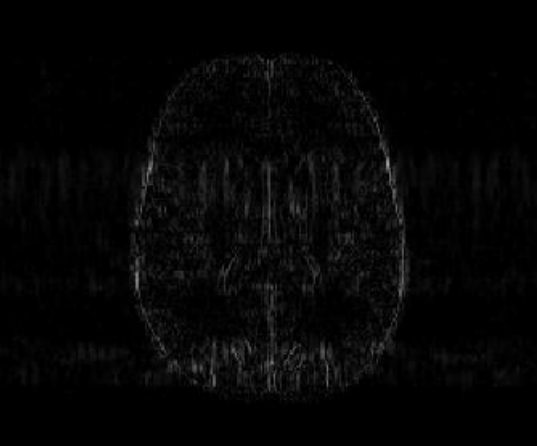
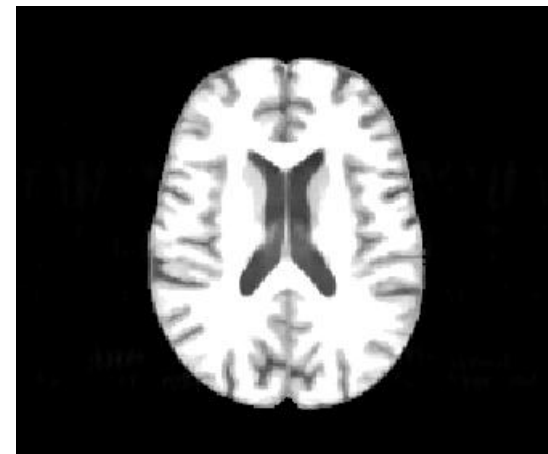


Lustig *et al.*  9.4 %
 M-FOCUSS  3.2 %

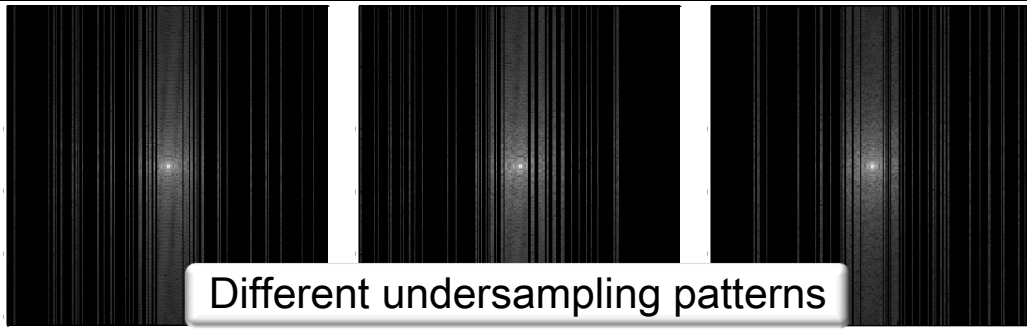
k-space, 25 % of Nyquist rate






M-FOCUSS¹ Error: 3.2 % RMSE



[1] Cotter *et al.* T Signal Proces, 2005

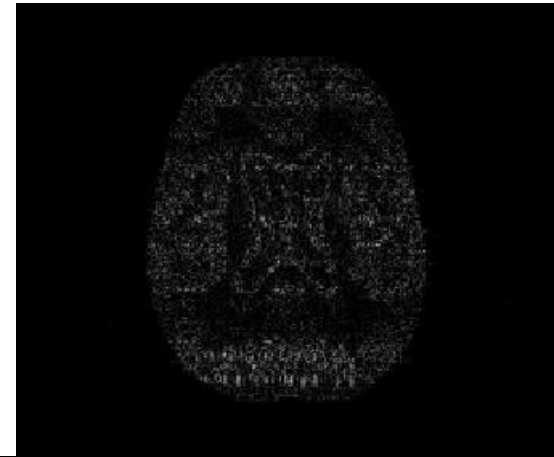
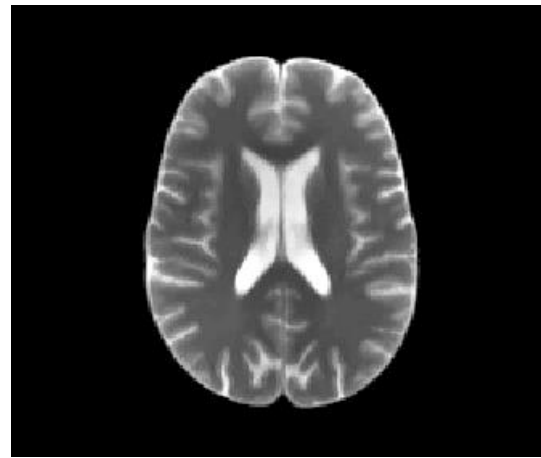


Lustig <i>et al.</i>		9.4 %
M-FOCUSS		3.2 %
Joint Bayes		2.3 %

k-space, 25 % of Nyquist rate



Our Bayesian CS Error: 2.3 % RMSE



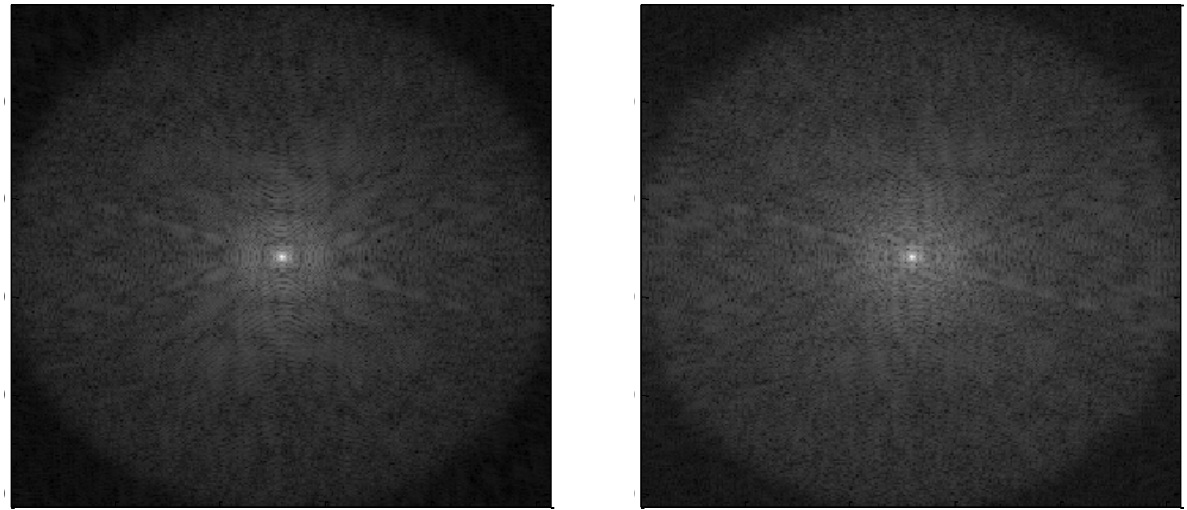
0.7

0

0.15

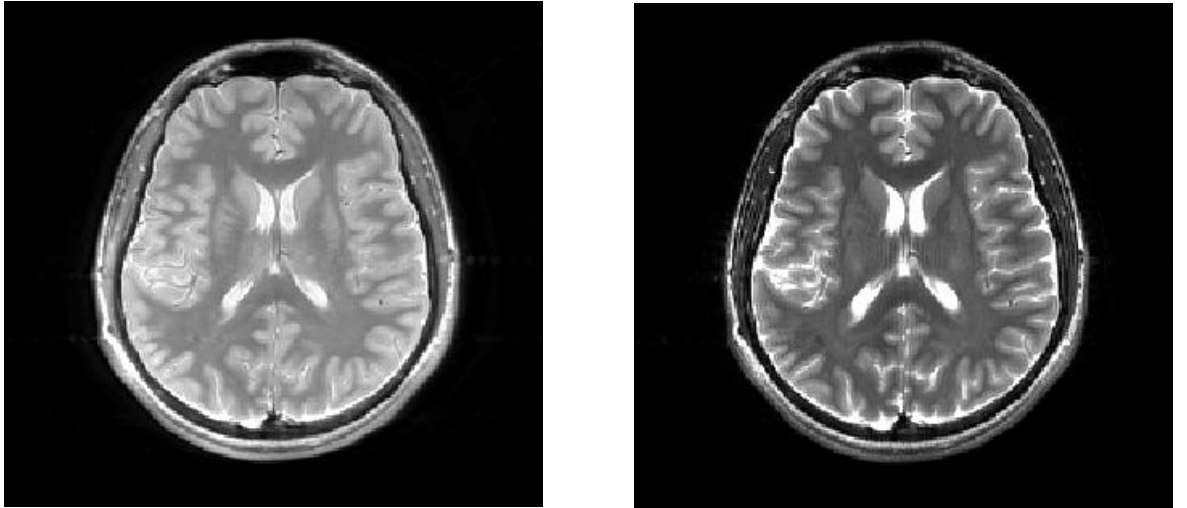
0

TSE Scans : *in vivo* acquisition



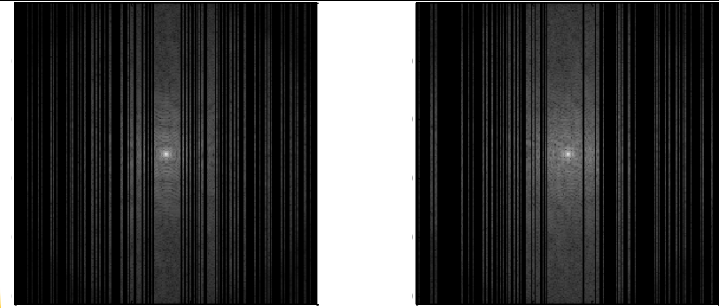
k-space
100 % of Nyquist rate

Inverse FFT



Error: 0 % RMSE

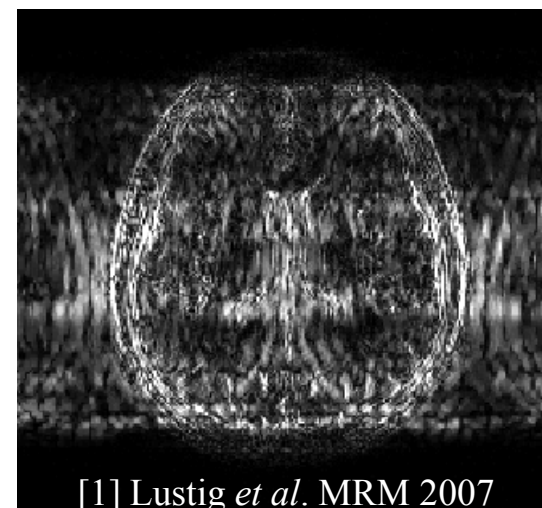
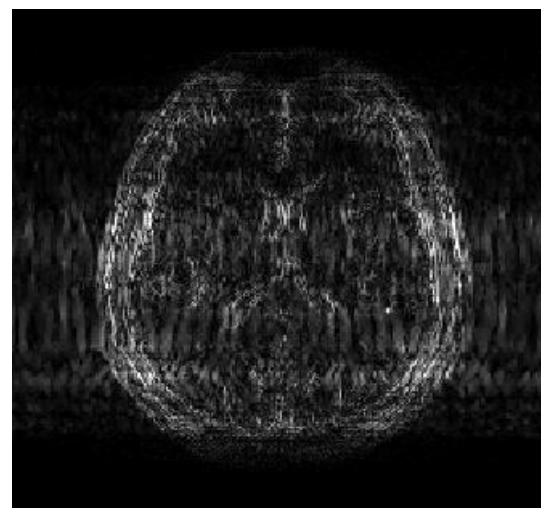
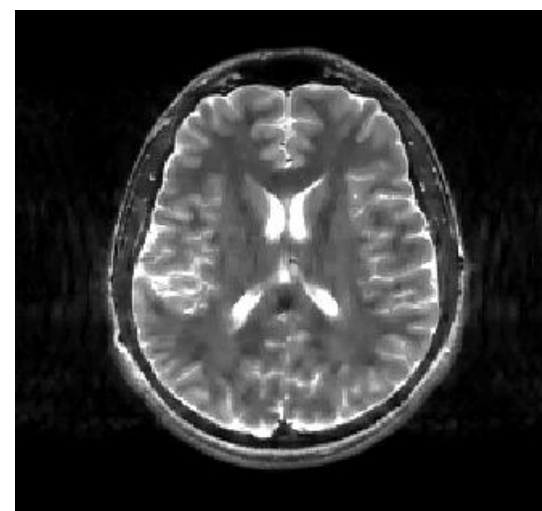
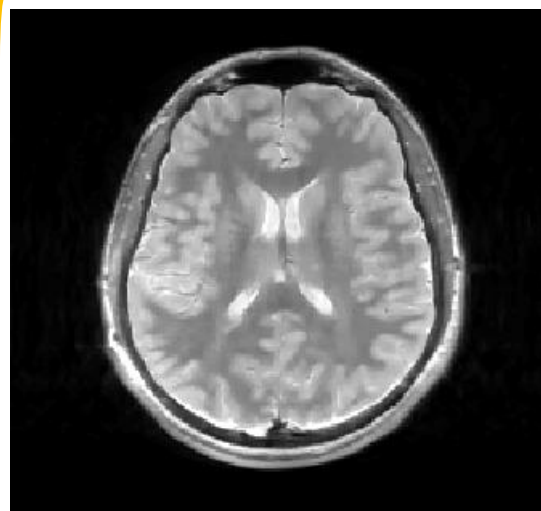
Lustig *et al.* 9.4 %



k -space, 40 % of Nyquist rate

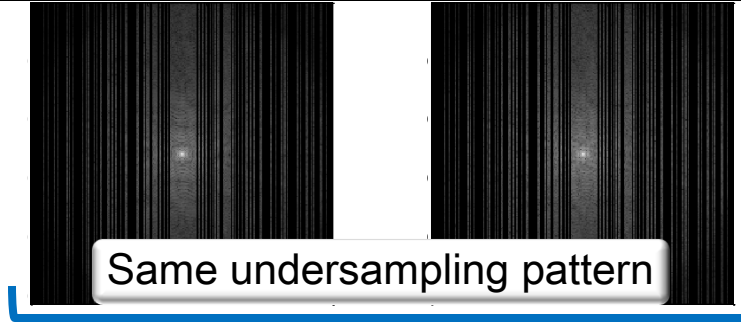


Lustig *et al.*¹



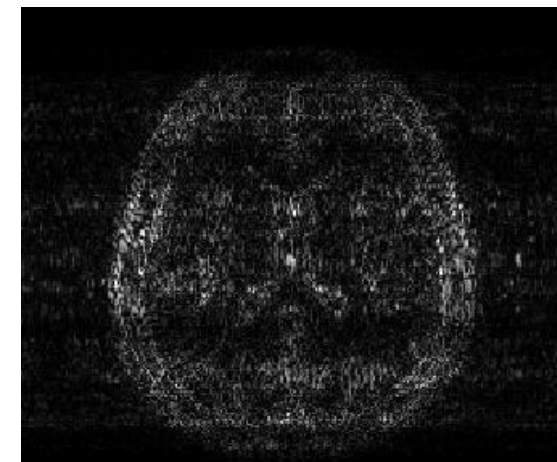
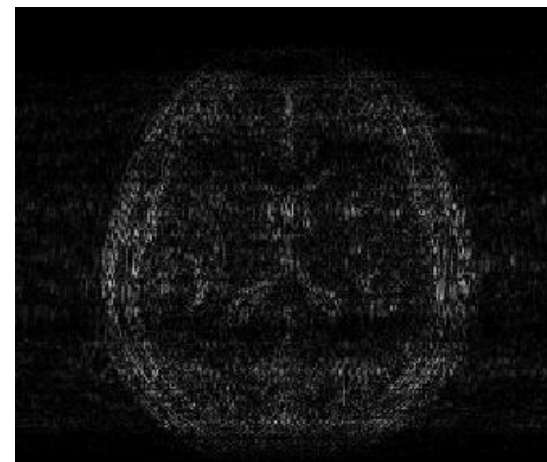
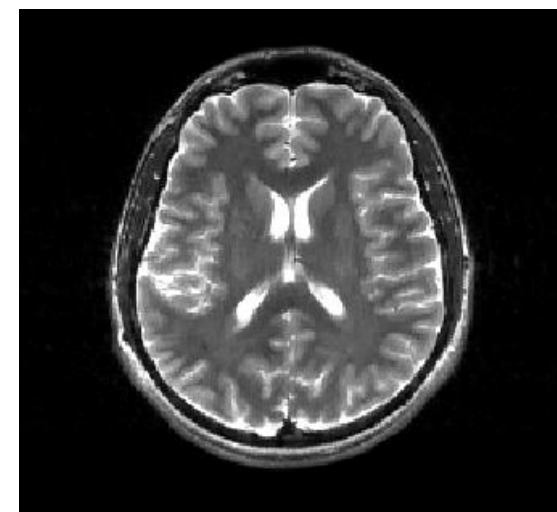
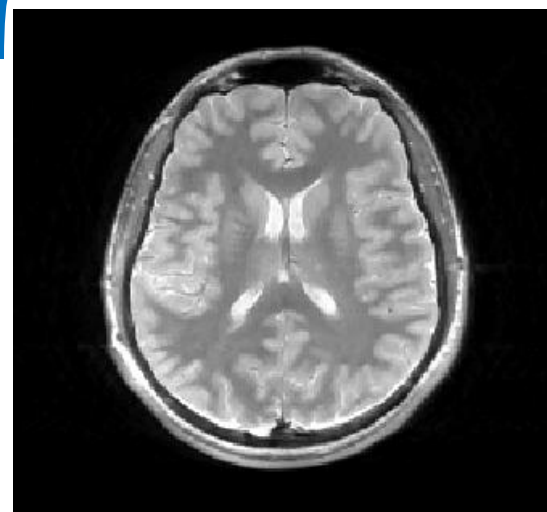
Error: 9.4 % RMSE

Lustig *et al.* 9.4 %
M-FOCUSS 5.1 %






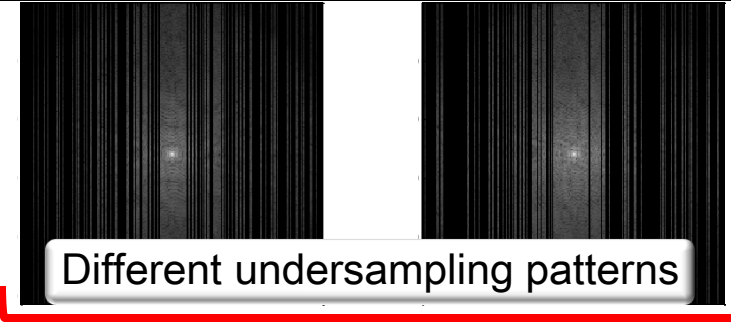
k-space, 40 % of Nyquist rate

M-FOCUSS¹



Error: 5.1 % RMSE

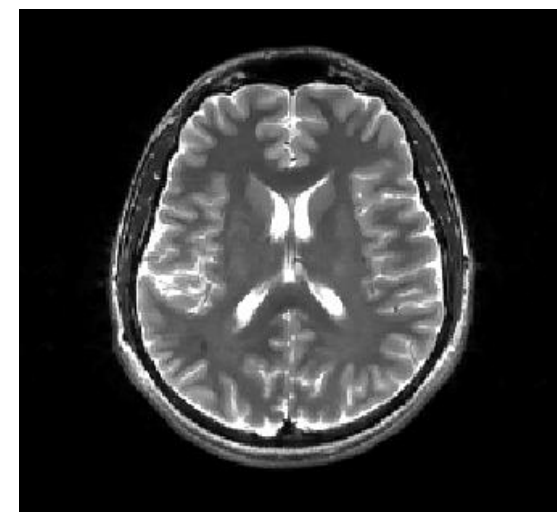
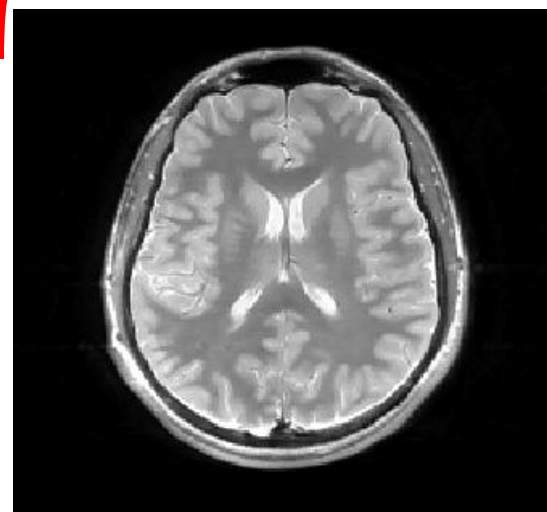
Lustig <i>et al.</i>		9.4 %
M-FOCUSS		5.1 %
Joint Bayes		3.6 %



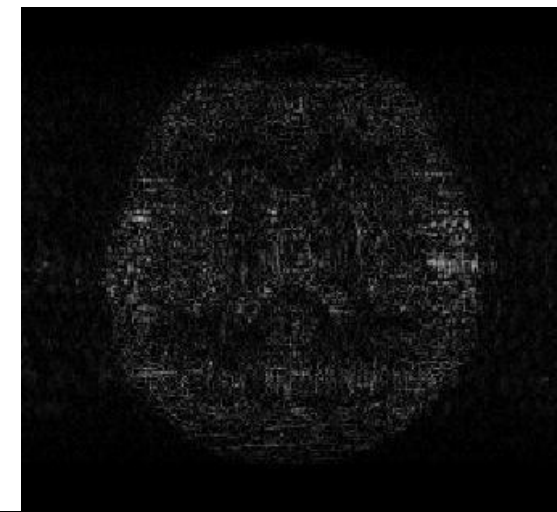
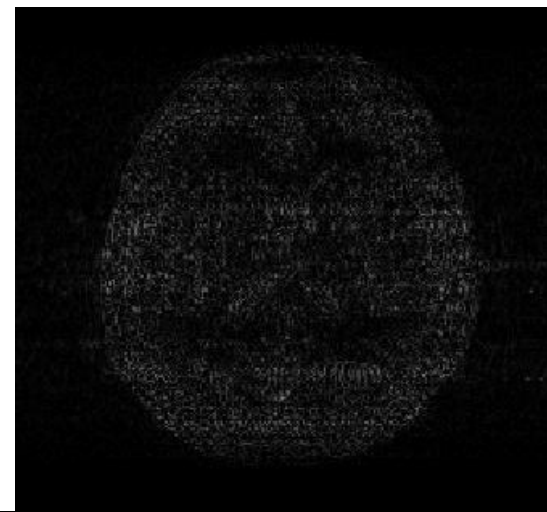
Different undersampling patterns

k-space, 40 % of Nyquist rate

Our Bayesian CS



Error: 3.6 % RMSE



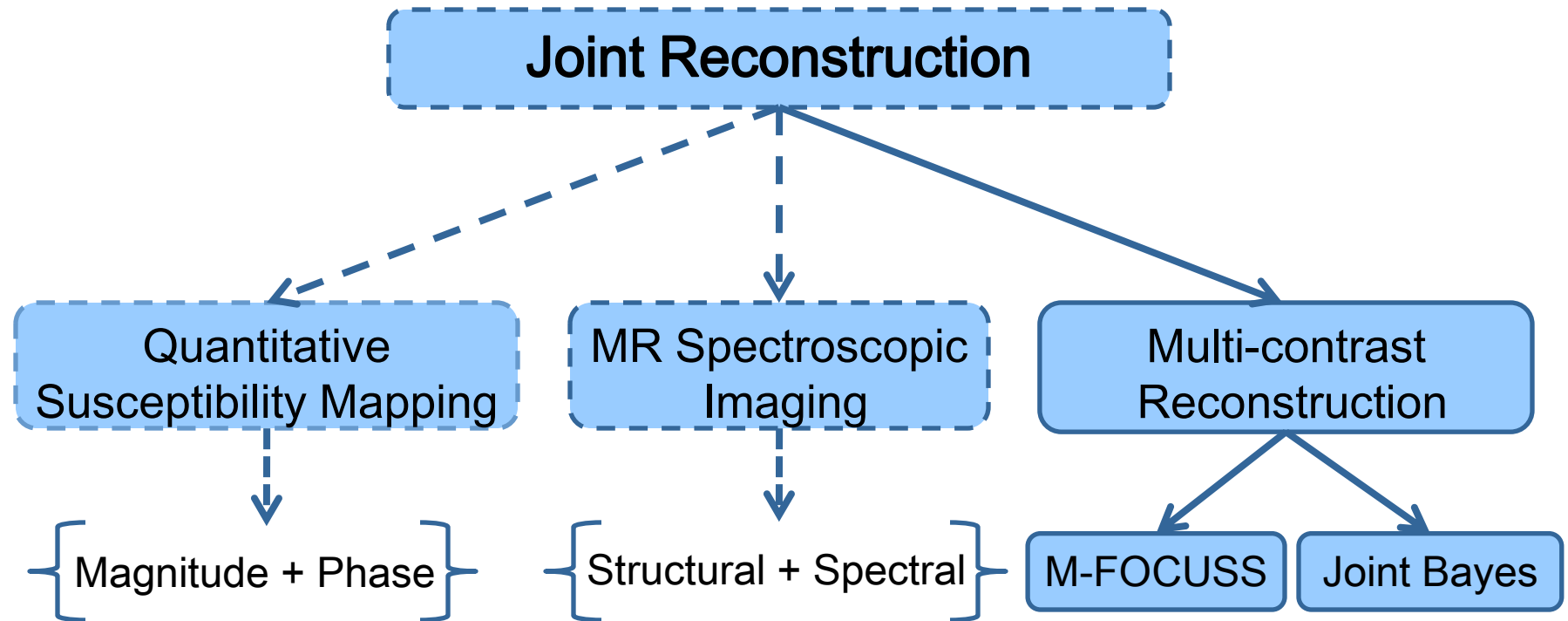
Extensions and Limitations

- ❖ We assumed the multi-contrast images to be real-valued. Extension to complex-valued images is possible by using a mirror-symmetric sampling pattern and separating real and imaginary parts of the images.

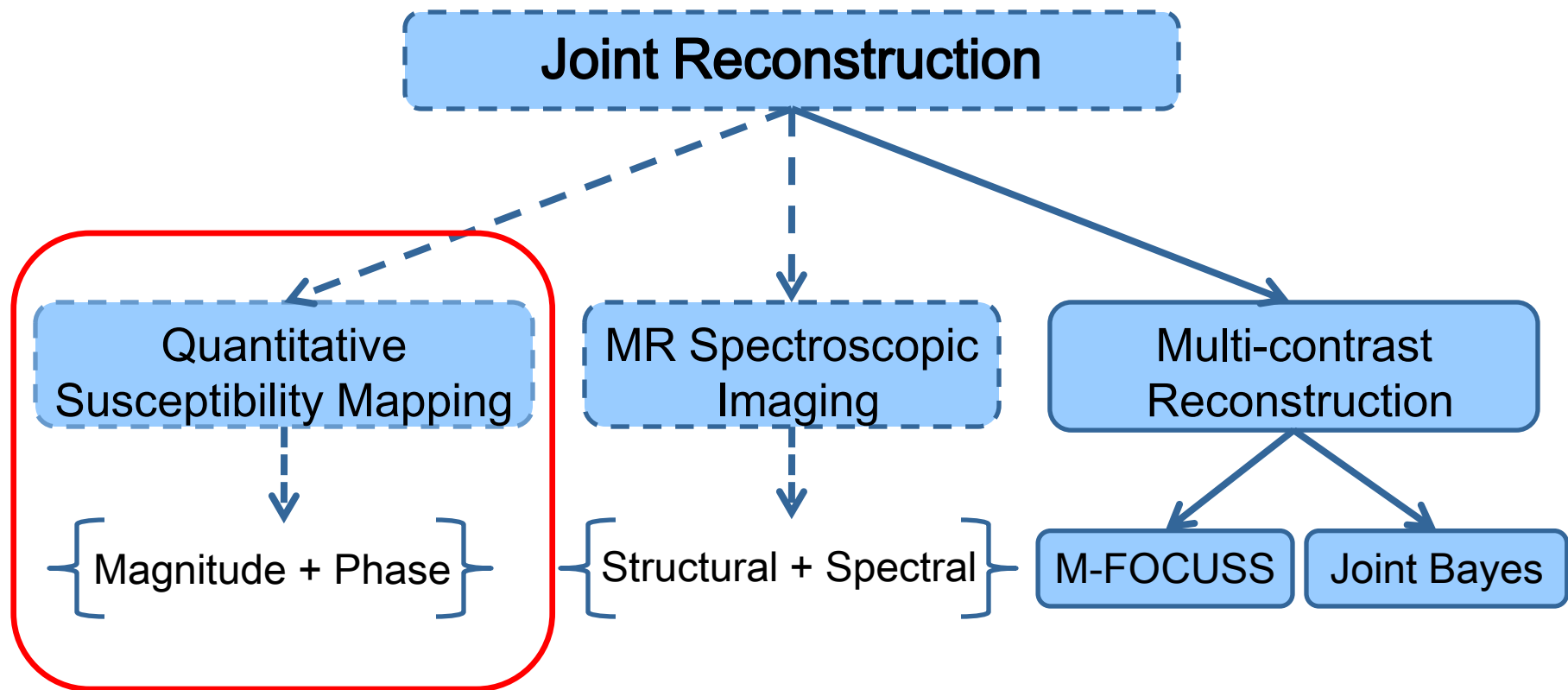
Extensions and Limitations

- ❖ We assumed the multi-contrast images to be real-valued. Extension to complex-valued images is possible by using a mirror-symmetric sampling pattern and separating real and imaginary parts of the images.
- ❖ Whereas the other two methods take under an hour, the Bayesian method takes about **20 hours** with this initial implementation.
- ❖ Current work is on increasing the reconstruction speed using
 - Graphics Processing Cards (GPUs) on the hardware front, and
 - Employing variational Bayesian analysis on the algorithm front

Other applications of joint reconstruction



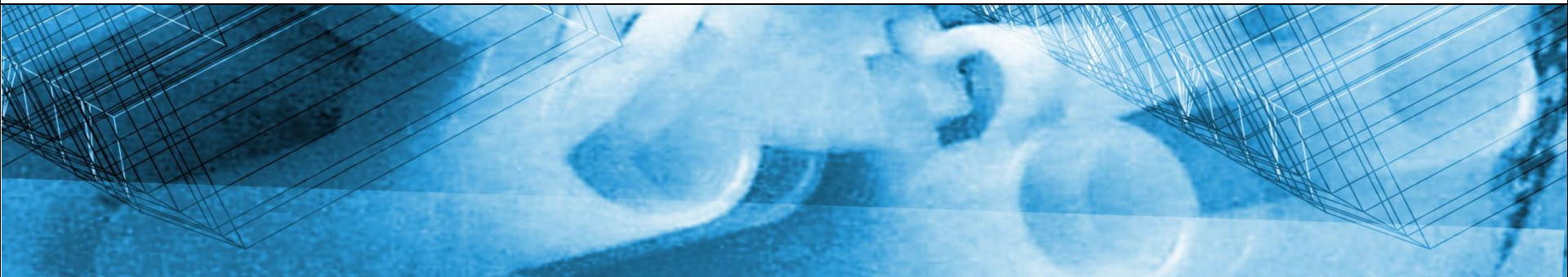
Other applications of joint reconstruction



Next topic

Conclusion

- ❖ We presented two joint reconstruction algorithms, M-FOCUSS and joint Bayesian CS, that significantly improved reconstruction quality of multi-contrast images from undersampled data.
- ❖ While joint Bayesian method reduced reconstruction errors by up to 4 times relative to a popular CS algorithm¹, current implementation suffers from long reconstruction times.
- ❖ M-FOCUSS is a notable candidate that trades off reconstruction quality and processing speed.



Quantitative Susceptibility Mapping with Magnitude Prior

Berkin Bilgic¹, Audrey P. Fan¹, Elfar Adalsteinsson^{1,2}

¹EECS, MIT, Cambridge, MA, United States

²Harvard-MIT Division of Health Sciences and Technology, Cambridge, MA, United States

Quantitative Susceptibility Mapping (QSM)

- Quantitative Susceptibility Mapping (QSM) aims to quantify tissue magnetic susceptibility with applications such as,
 - ❖ Tissue contrast enhancement¹
 - ❖ Estimation of venous blood oxygenation²
 - ❖ Quantification of tissue iron concentration³

Quantitative Susceptibility Mapping (QSM)

- Quantitative Susceptibility Mapping (QSM) aims to quantify tissue magnetic susceptibility with applications such as,
 - ❖ Tissue contrast enhancement¹
 - ❖ Estimation of venous blood oxygenation²
 - ❖ Quantification of tissue iron concentration³
- Estimation of the susceptibility map χ from the unwrapped phase φ involves solving an inverse problem,

$$\delta = \mathbf{F}^{-1} \mathbf{D} \mathbf{F} \chi$$

F: Discrete Fourier Transform matrix

D: susceptibility kernel in k -space

$$\delta = \frac{\varphi}{\gamma \cdot \mathbf{TE} \cdot \mathbf{B}_0} : \text{normalized field map}$$

Quantitative Susceptibility Mapping (QSM)

- Quantitative Susceptibility Mapping (QSM) aims to quantify tissue magnetic susceptibility with applications such as,
 - ❖ Tissue contrast enhancement¹
 - ❖ Estimation of venous blood oxygenation²
 - ❖ Quantification of tissue iron concentration³
- Estimation of the susceptibility map χ from the unwrapped phase φ involves solving an inverse problem,

$$\delta = \mathbf{F}^{-1} \mathbf{D} \mathbf{F} \chi$$

measured

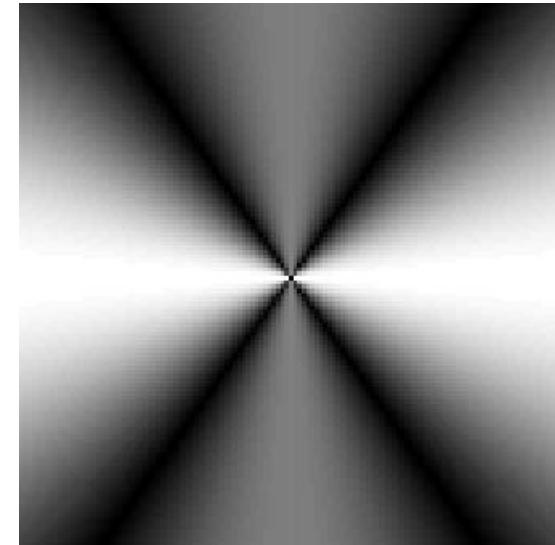
to be estimated

Quantitative Susceptibility Mapping (QSM)

- Quantitative Susceptibility Mapping (QSM) aims to quantify tissue magnetic susceptibility with applications such as,
 - ❖ Tissue contrast enhancement¹
 - ❖ Estimation of venous blood oxygenation²
 - ❖ Quantification of tissue iron concentration³
- Estimation of the susceptibility map χ from the unwrapped phase φ involves solving an inverse problem, $\delta = \mathbf{F}^{-1}\mathbf{D}\mathbf{F}\chi$
- The inversion is made difficult by zeros on a conical surface in susceptibility kernel \mathbf{D}

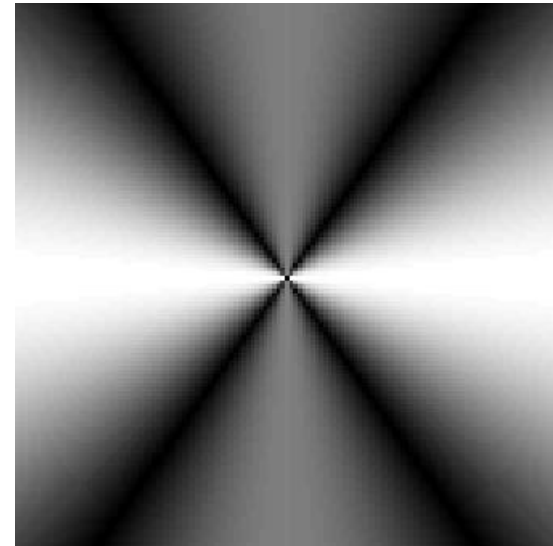
$$\mathbf{D} = \left(\begin{array}{c} 1 \\ 3 - \frac{k_z^2}{k^2} \end{array} \right)$$

$|\mathbf{D}|$



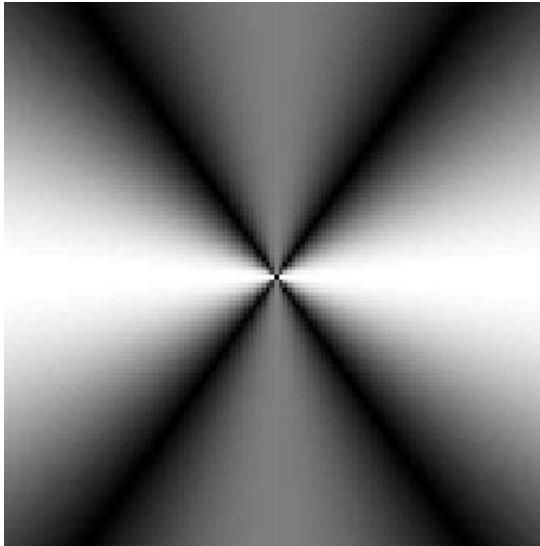
Regularized Inversion for QSM

|D|

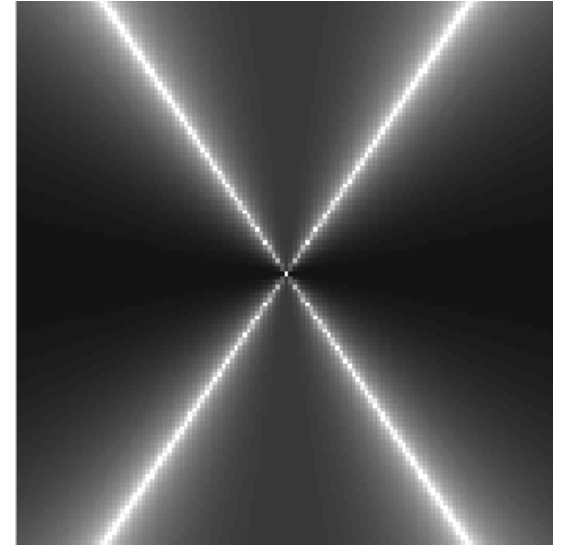


Regularized Inversion for QSM

$|\mathbf{D}|$



$\log|\mathbf{D}^{-1}|$

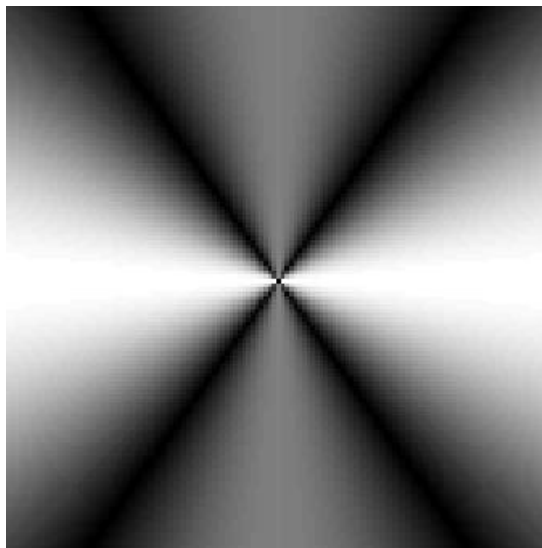


$$\mathbf{F}\mathbf{D}^{-1}\mathbf{F}\delta = \chi$$

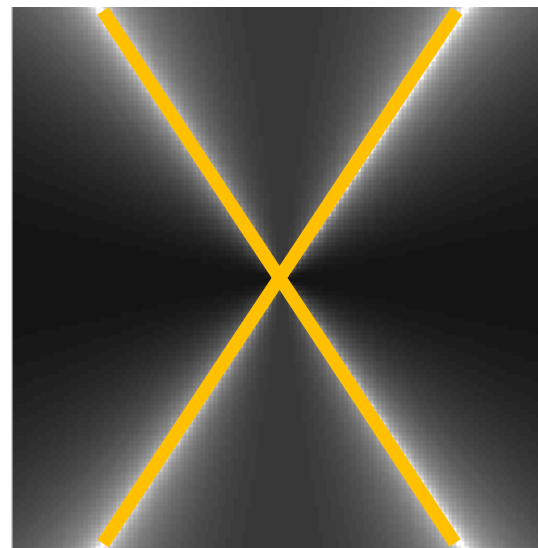
- Solving for χ by convolving with the inverse of \mathbf{D} is not possible, as it diverges along the magic angle

Regularized Inversion for QSM

$|\mathbf{D}|$



$\log|\mathbf{D}^{-1}|$

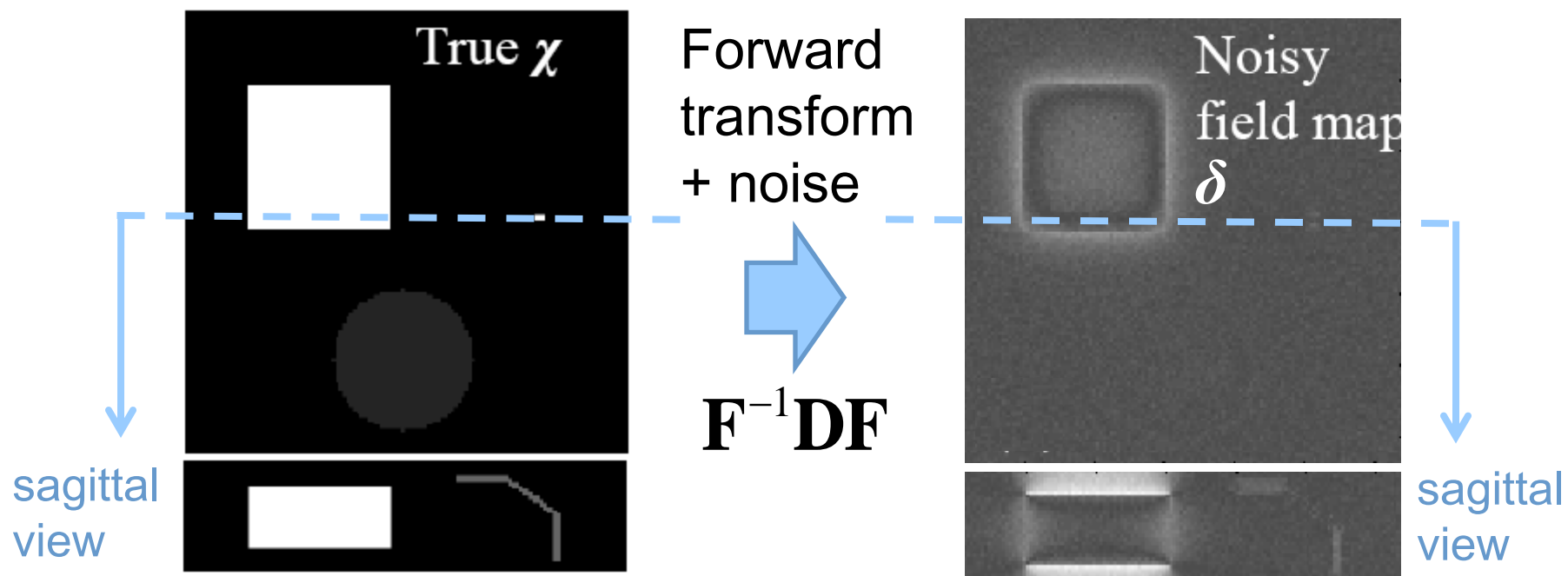


~~$\mathbf{F}\mathbf{D}^{-1}\mathbf{F}^H = \chi$~~

diverges to ∞

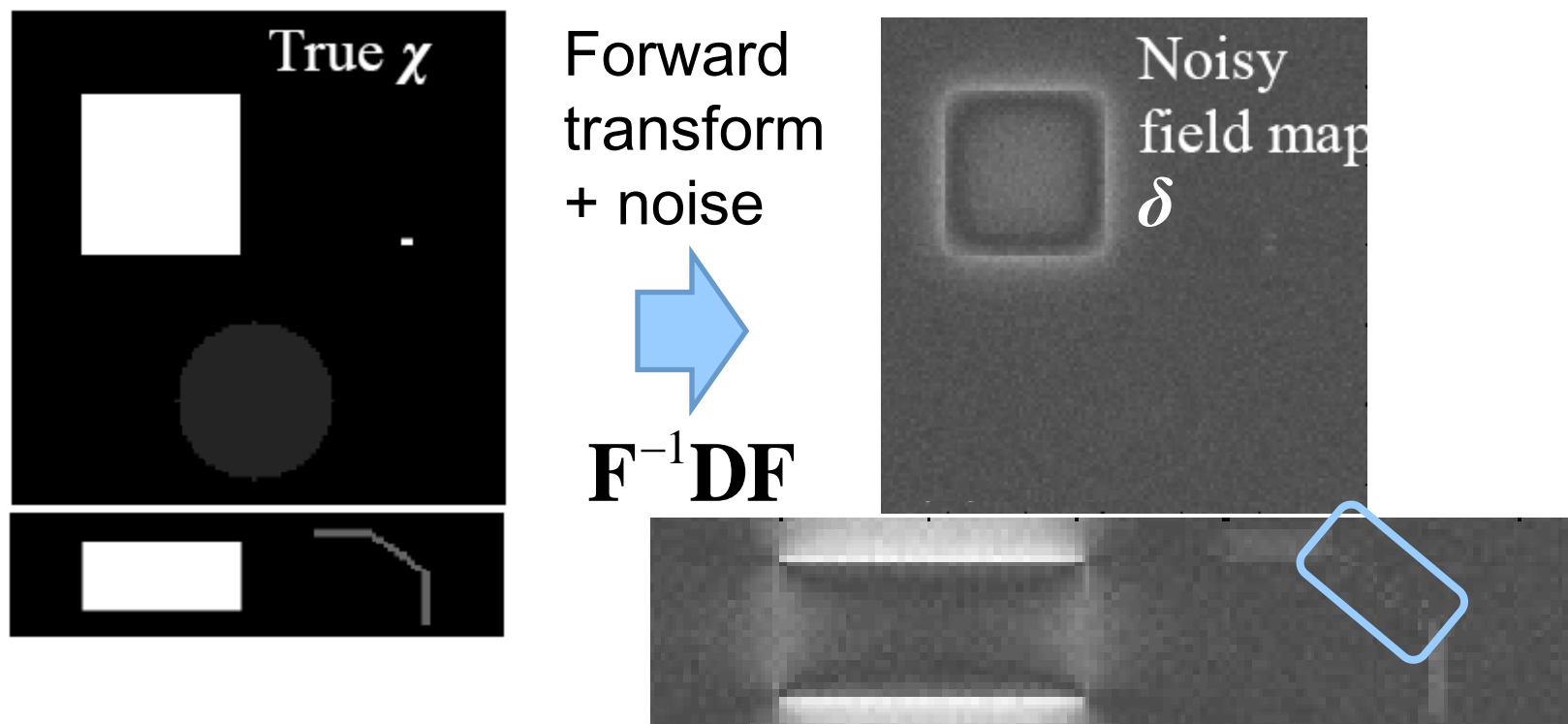
- Solving for χ by convolving with the inverse of \mathbf{D} is not possible, as it diverges along the magic angle

Regularized Inversion for QSM

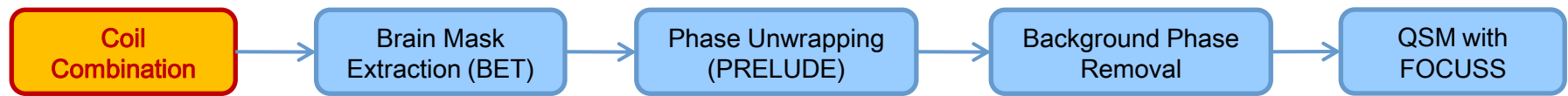


- Solving for χ by convolving with the inverse of \mathbf{D} is not possible, as it diverges along the magic angle
- Spatial details that have frequency components at the magic angle lose conspicuity in the field map δ

Regularized Inversion for QSM

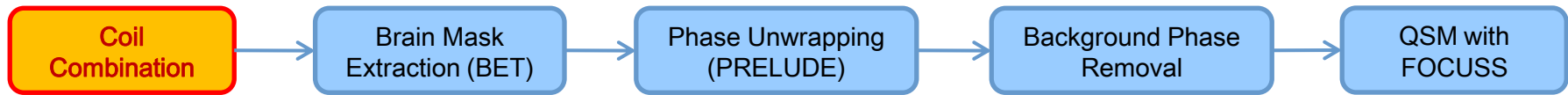


- Solving for χ by convolving with the inverse of \mathbf{D} is not possible, as it diverges along the magic angle
- Spatial details that have frequency components at the magic angle lose conspicuity in the field map δ
- We propose to use regularization to facilitate the inversion



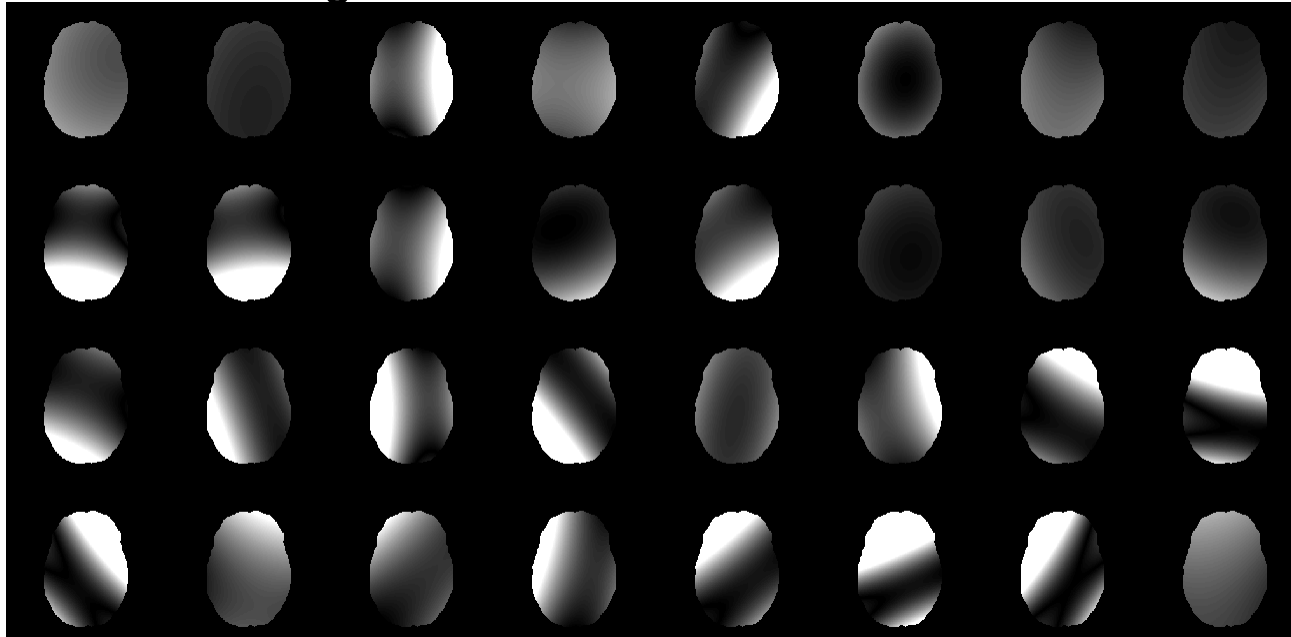
Phase-aware Coil Combination

- 3D GRE acquisition with phased array coils and body coil
- Normalize each channel image with the body coil

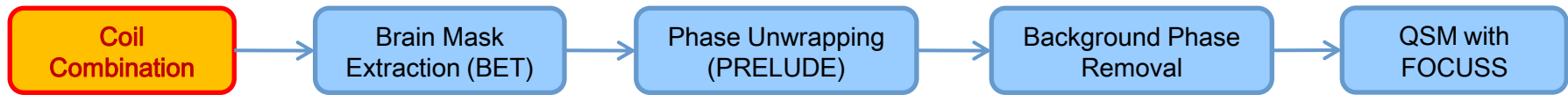


Phase-aware Coil Combination

magnitudes of the coil sensitivities

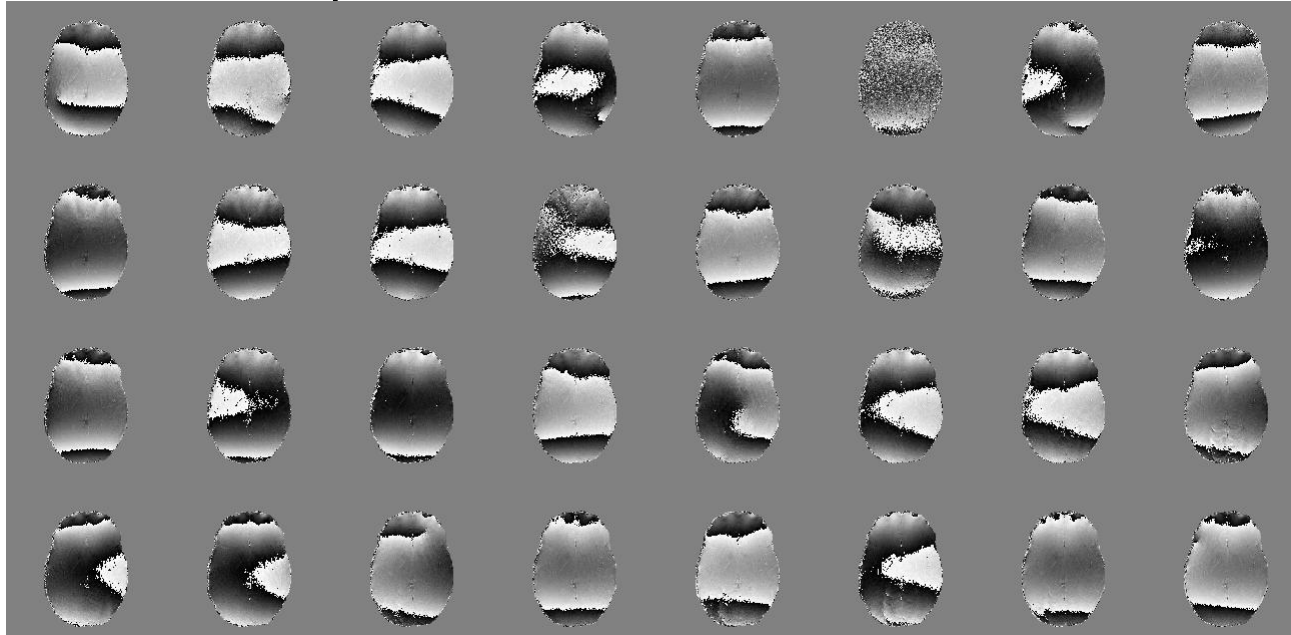


- 3D GRE acquisition with phased array coils and body coil
- Normalize each channel image with the body coil
- Fit 2nd order polynomials to the magnitude of the normalized images → magnitude of the coil sensitivities

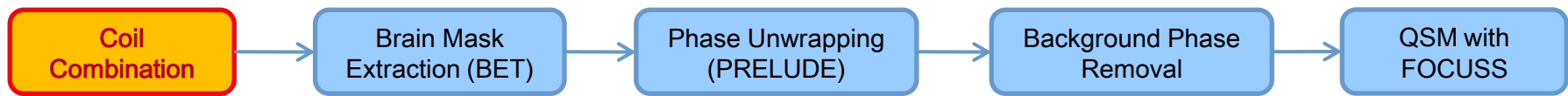


Phase-aware Coil Combination

phase of the coil sensitivities

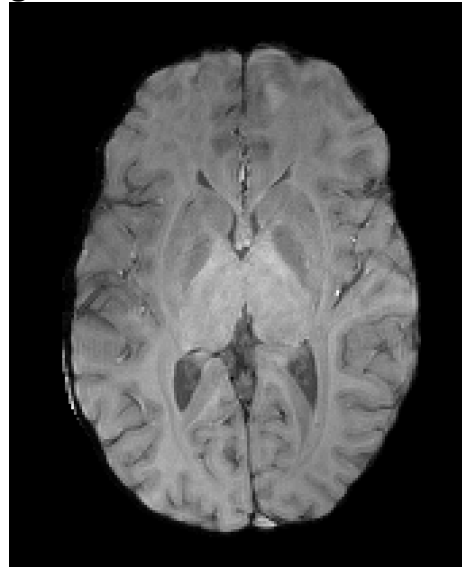


- 3D GRE acquisition with phased array coils and body coil
- Normalize each channel image with the body coil
- Fit 2nd order polynomials to the magnitude of the normalized images → magnitude of the coil sensitivities
- Phase of the normalized images → phase of the coil sensitivities

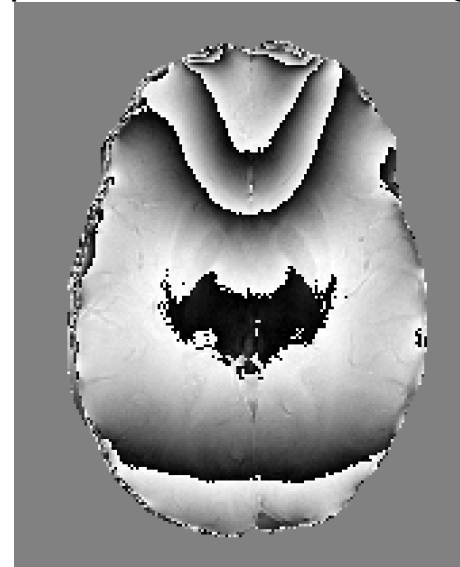


Phase-aware Coil Combination

magnitude of combined image



phase of combined image

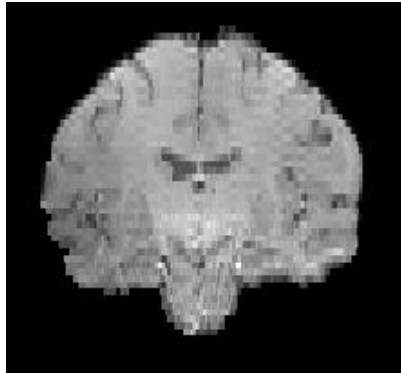


- 3D GRE acquisition with phased array coils and body coil
- Normalize each channel image with the body coil
- Fit 2nd order polynomials to the magnitude of the normalized images → magnitude of the coil sensitivities
- Phase of the normalized images → phase of the coil sensitivities
- Final image is obtained by least-squares coil combination



Brain Mask Extraction & Phase Unwrapping

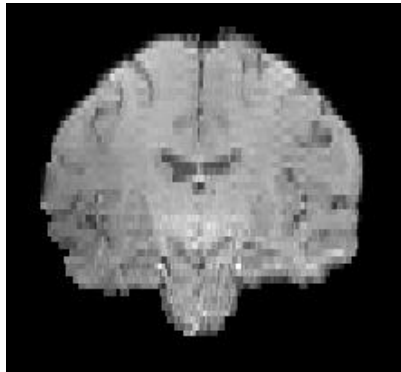
- Brain mask was generated with the FSL Brain Extraction Tool¹



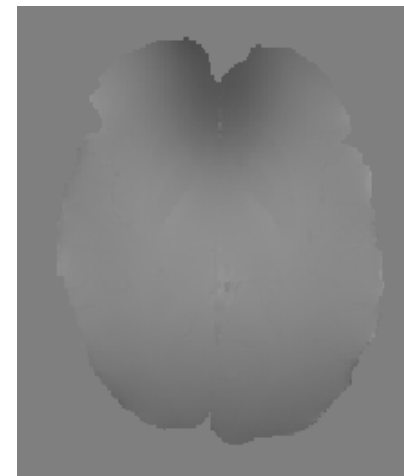
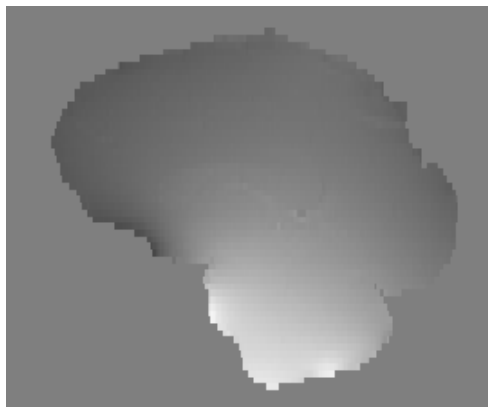
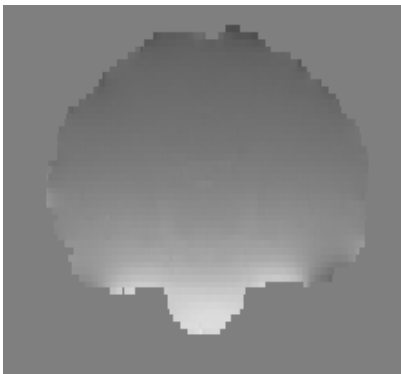


Brain Mask Extraction & Phase Unwrapping

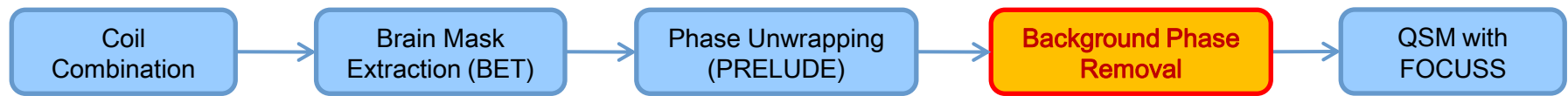
- Brain mask was generated with the FSL Brain Extraction Tool¹



- Phase unwrapping was done with the FSL PRELUDE²

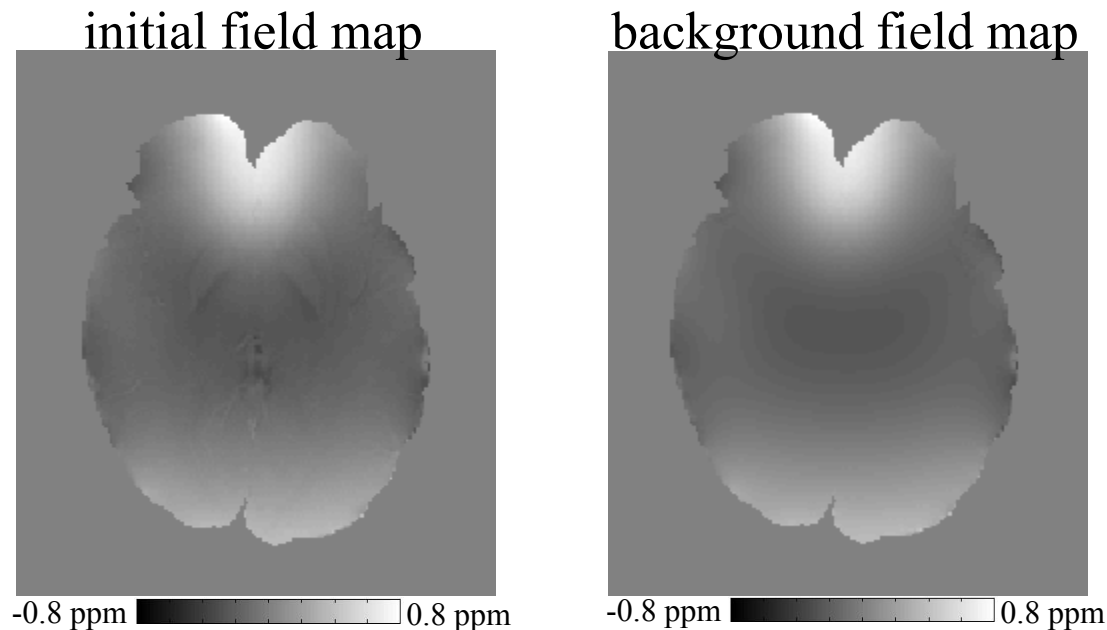


¹ Smith SM, Hum. Brain Mapp. 2002 ² Jenkinson M, MRM 2003

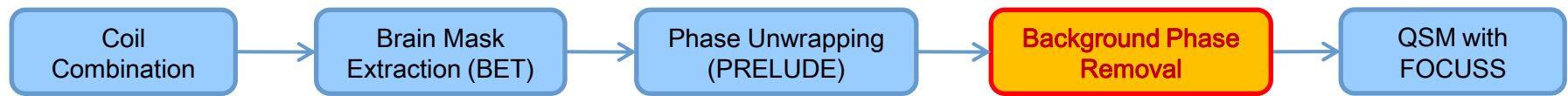


Background Phase Removal

- The background phase was estimated with the Effective Dipole Fitting method¹

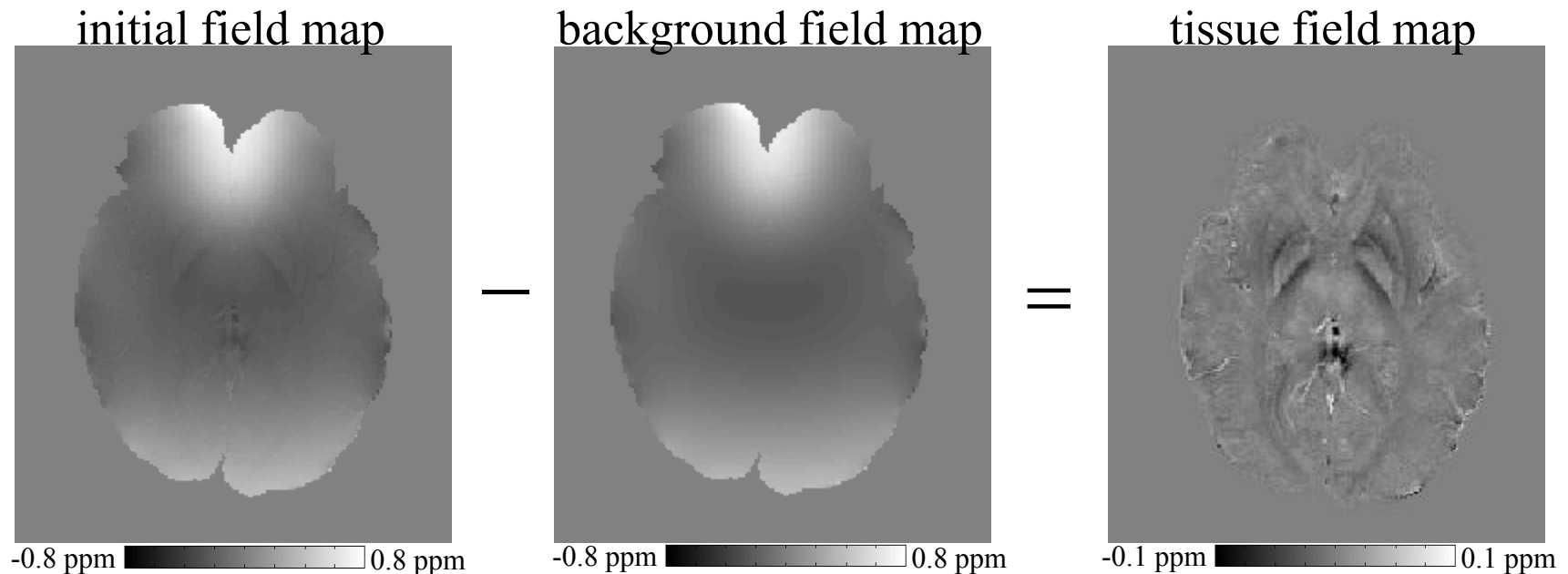


¹ Liu T *et al.*, ISMRM 2010

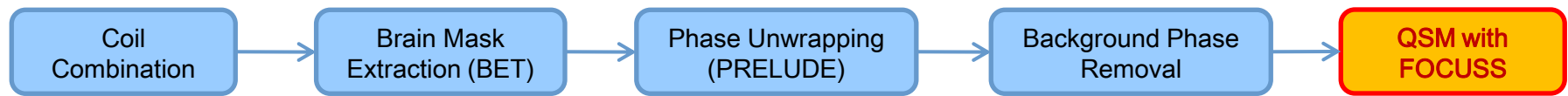


Background Phase Removal

- The background phase was estimated with the Effective Dipole Fitting method¹
- Subtracting the estimated background from the initial field map gives the tissue field map



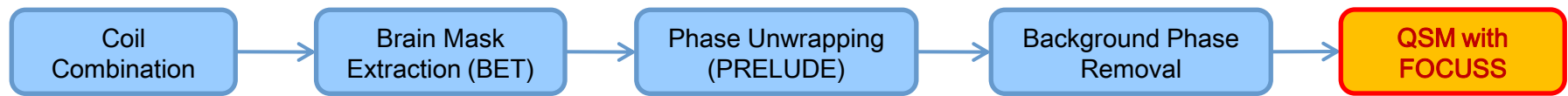
¹ Liu T *et al.*, ISMRM 2010



FOCUSS-QSM with magnitude prior

- The tissue field map δ is related to the susceptibility distribution χ via

$$\delta = \mathbf{F}^{-1} \mathbf{D} \mathbf{F} \chi$$



FOCUSS-QSM with magnitude prior

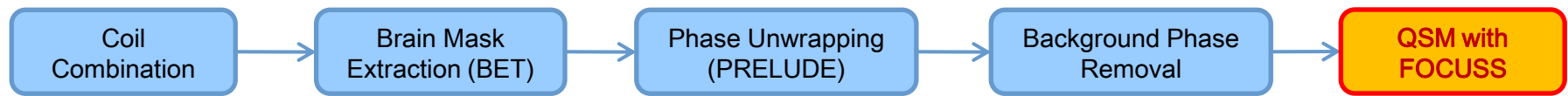
- The tissue field map δ is related to the susceptibility distribution χ via

$$\delta = \mathbf{F}^{-1} \mathbf{D} \mathbf{F} \chi$$

- Multiplying both sides with $\mathbf{V}_x \mathbf{F}$

$$\mathbf{V}_x \mathbf{F} \delta = \mathbf{V}_x \mathbf{D} \mathbf{F} \chi$$

where \mathbf{V}_x is a diagonal matrix with $\mathbf{V}_x(\omega, \omega) = (1 - e^{-2\pi j \omega / n})$



FOCUSS-QSM with magnitude prior

- The tissue field map δ is related to the susceptibility distribution χ via

$$\delta = \mathbf{F}^{-1} \mathbf{D} \mathbf{F} \chi$$

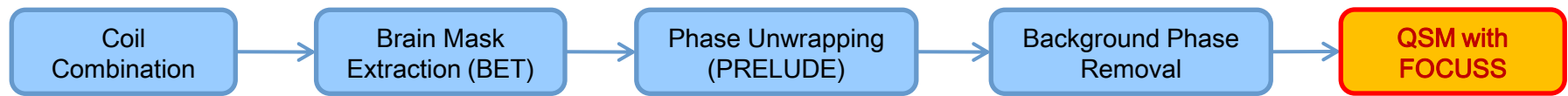
- Multiplying both sides with $\mathbf{V}_x \mathbf{F}$

$$\mathbf{V}_x \mathbf{F} \delta = \mathbf{V}_x \mathbf{D} \mathbf{F} \chi$$

where \mathbf{V}_x is a diagonal matrix with $\mathbf{V}_x(\omega, \omega) = (1 - e^{-2\pi j \omega / n})$

- This corresponds to taking the spatial gradient along the x axis

$$\mathbf{F}(\partial_x \delta) = \mathbf{D} \mathbf{F}(\partial_x \chi)$$



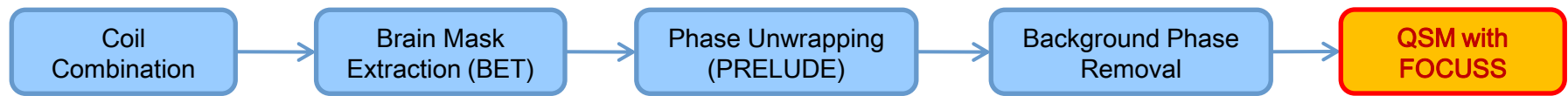
FOCUSS-QSM with magnitude prior

- The gradient of the tissue field map δ is related to the gradient of the susceptibility distribution χ via

$$\mathbf{F}(\partial_x \delta) = \mathbf{DF}(\partial_x \chi)$$

- We solve for $\partial_x \chi$ with the FOCUSS algorithm¹ at k^{th} iteration,

$$\mathbf{W}_k = \text{diag}\left(|\partial_x \chi_{k-1}|^{1/2}\right)$$



FOCUSS-QSM with magnitude prior

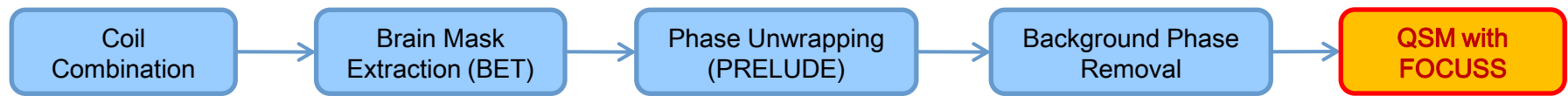
- The gradient of the tissue field map δ is related to the gradient of the susceptibility distribution χ via

$$\mathbf{F}(\partial_x \delta) = \mathbf{DF}(\partial_x \chi)$$

- We solve for $\partial_x \chi$ with the FOCUSS algorithm¹ at k^{th} iteration,

$$\mathbf{W}_k = \text{diag}\left(|\partial_x \chi_{k-1}|^{1/2}\right)$$

$$\mathbf{q}_k = \underset{\mathbf{q}}{\text{argmin}} \left\| \mathbf{F}(\partial_x \delta) - \mathbf{DFW}_k \mathbf{q} \right\|_2^2 + \lambda \|\mathbf{q}\|_2^2$$



FOCUSS-QSM with magnitude prior

- The gradient of the tissue field map δ is related to the gradient of the susceptibility distribution χ via

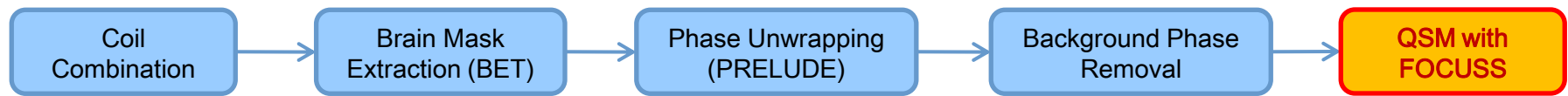
$$\mathbf{F}(\partial_x \delta) = \mathbf{DF}(\partial_x \chi)$$

- We solve for $\partial_x \chi$ with the FOCUSS algorithm¹ at k^{th} iteration,

$$\mathbf{W}_k = \text{diag}\left(|\partial_x \chi_{k-1}|^{1/2}\right)$$

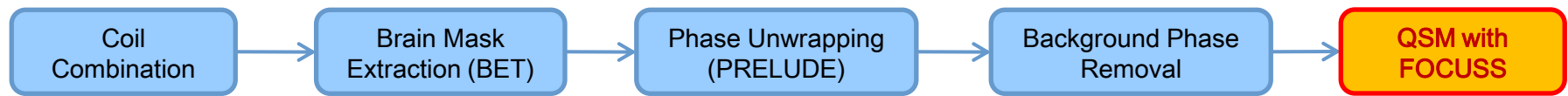
$$\mathbf{q}_k = \underset{\mathbf{q}}{\text{argmin}} \left\| \mathbf{F}(\partial_x \delta) - \mathbf{DFW}_k \mathbf{q} \right\|_2^2 + \lambda \|\mathbf{q}\|_2^2$$

$$\partial_x \chi_k = \mathbf{W}_k \mathbf{q}_k$$



FOCUSS-QSM with magnitude prior

- We expect the susceptibility distribution to share similar spatial gradients as the magnitude image.



FOCUSS-QSM with magnitude prior

- We expect the susceptibility distribution to share similar spatial gradients as the magnitude image.
- To impose this prior, we modify the update equations as,

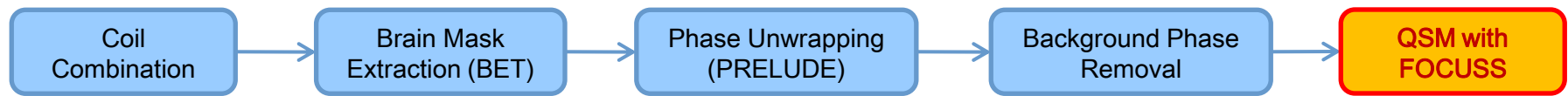
$$\mathbf{W}_{prior} = \text{diag}\left(|\partial_x m|^{1/2}\right), \quad m: \text{magnitude image}$$

at k^{th} iteration,

$$\mathbf{W}_k = \text{diag}\left(|\partial_x \chi_{k-1}|^{1/2}\right)$$

$$\mathbf{q}_k = \underset{q}{\text{argmin}} \left\| \mathbf{F}(\partial_x \delta) - \mathbf{DF} \mathbf{W}_{prior} \mathbf{W}_k \mathbf{q} \right\|_2^2 + \lambda \|\mathbf{q}\|_2^2$$

$$\partial_x \chi_k = \mathbf{W}_{prior} \mathbf{W}_k \mathbf{q}_k$$

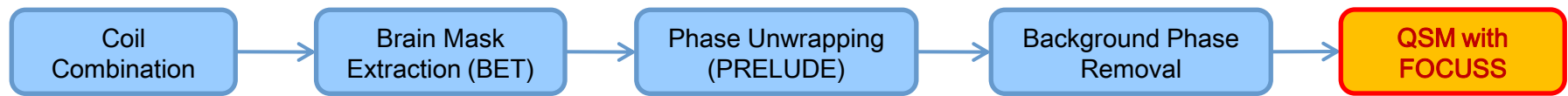


FOCUSS-QSM with magnitude prior

- We expect the susceptibility distribution to share similar spatial gradients as the magnitude image.
- Expressed in terms of $\partial_x \chi$,

$$\mathbf{W}_{prior} = \text{diag}\left(|\partial_x \mathbf{m}|^{1/2}\right), \quad \mathbf{m}: \text{magnitude image}$$

$$\partial_x \chi_k = \underset{\partial_x \chi}{\text{argmin}} \left\| \mathbf{F}(\partial_x \delta) - \mathbf{DF}(\partial_x \chi) \right\|_2^2 + \lambda \left\| \mathbf{W}_{prior}^{-1} \mathbf{W}_k^{-1} (\partial_x \chi) \right\|_2^2$$



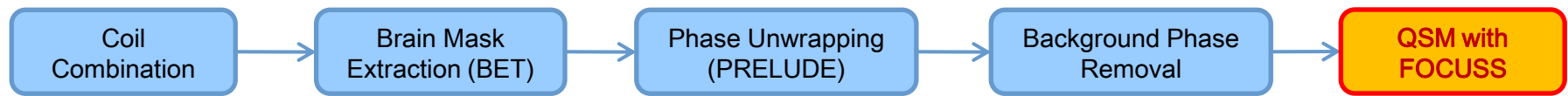
FOCUSS-QSM with magnitude prior

- We expect the susceptibility distribution to share similar spatial gradients as the magnitude image.
- Expressed in terms of $\partial_x \chi$,

$$\mathbf{W}_{prior} = \text{diag}\left(|\partial_x \mathbf{m}|^{1/2}\right), \quad \mathbf{m}: \text{magnitude image}$$

$$\partial_x \chi_k = \underset{\partial_x \chi}{\text{argmin}} \left\| \mathbf{F}(\partial_x \delta) - \mathbf{DF}(\partial_x \chi) \right\|_2^2 + \lambda \left\| \mathbf{W}_{prior}^{-1} \mathbf{W}_k^{-1} (\partial_x \chi) \right\|_2^2$$

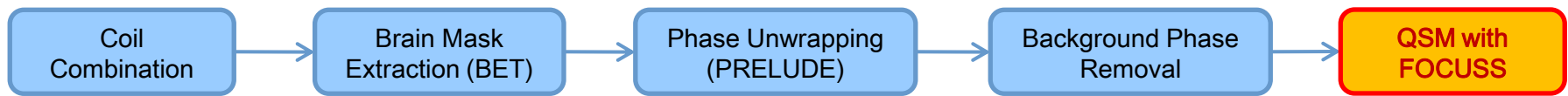
if $\partial_x \mathbf{m}_i$ is small, $\mathbf{W}_{prior}^{-1}(i,i)$ will be large and penalize $\partial_x \chi_i$ more



FOCUSS-QSM with magnitude prior

- After estimating the spatial gradients along x , y and z axes, the susceptibility distribution that matches these is found by solving a least squares problem,

$$\chi = \operatorname{argmin}_{\theta} \sum_{r=x,y,z} \|\partial_r \theta - \partial_r \chi\|_2^2 + \beta \cdot \|\delta - \mathbf{F}^{-1} \mathbf{D} \mathbf{F} \theta\|_2^2$$

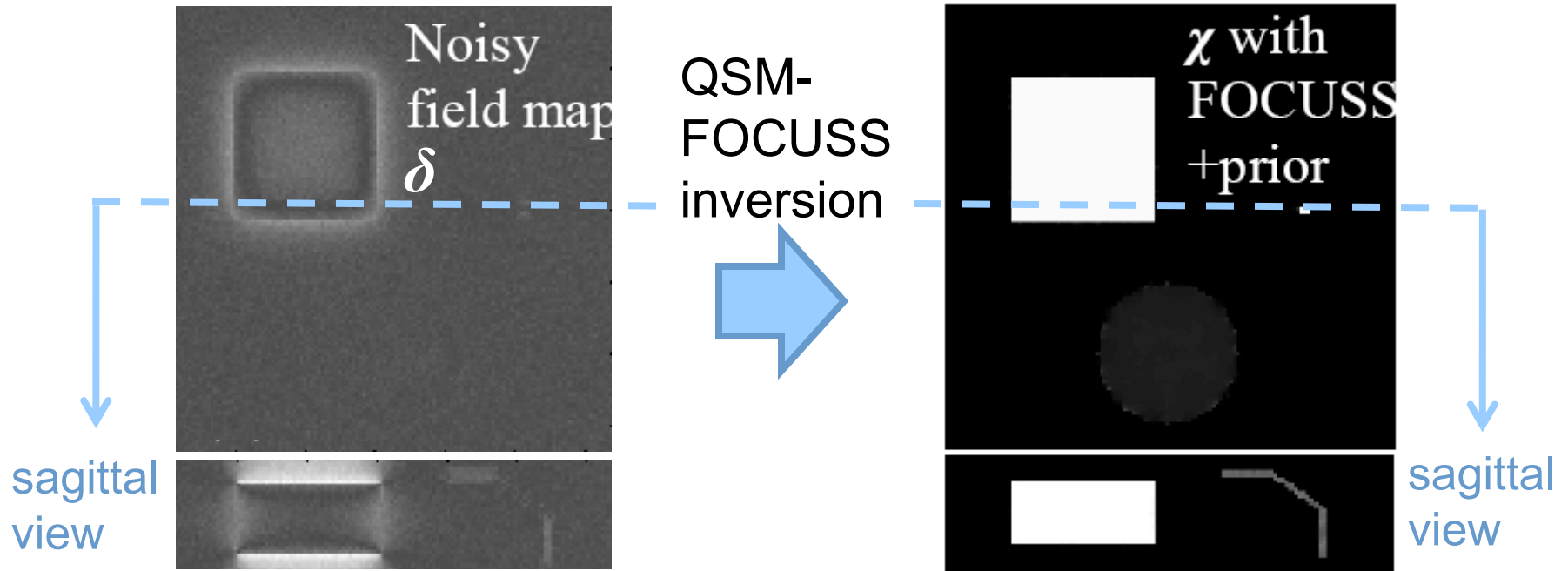


FOCUSS-QSM with magnitude prior

- After estimating the spatial gradients along x , y and z axes, the susceptibility distribution that matches these is found by solving a least squares problem,

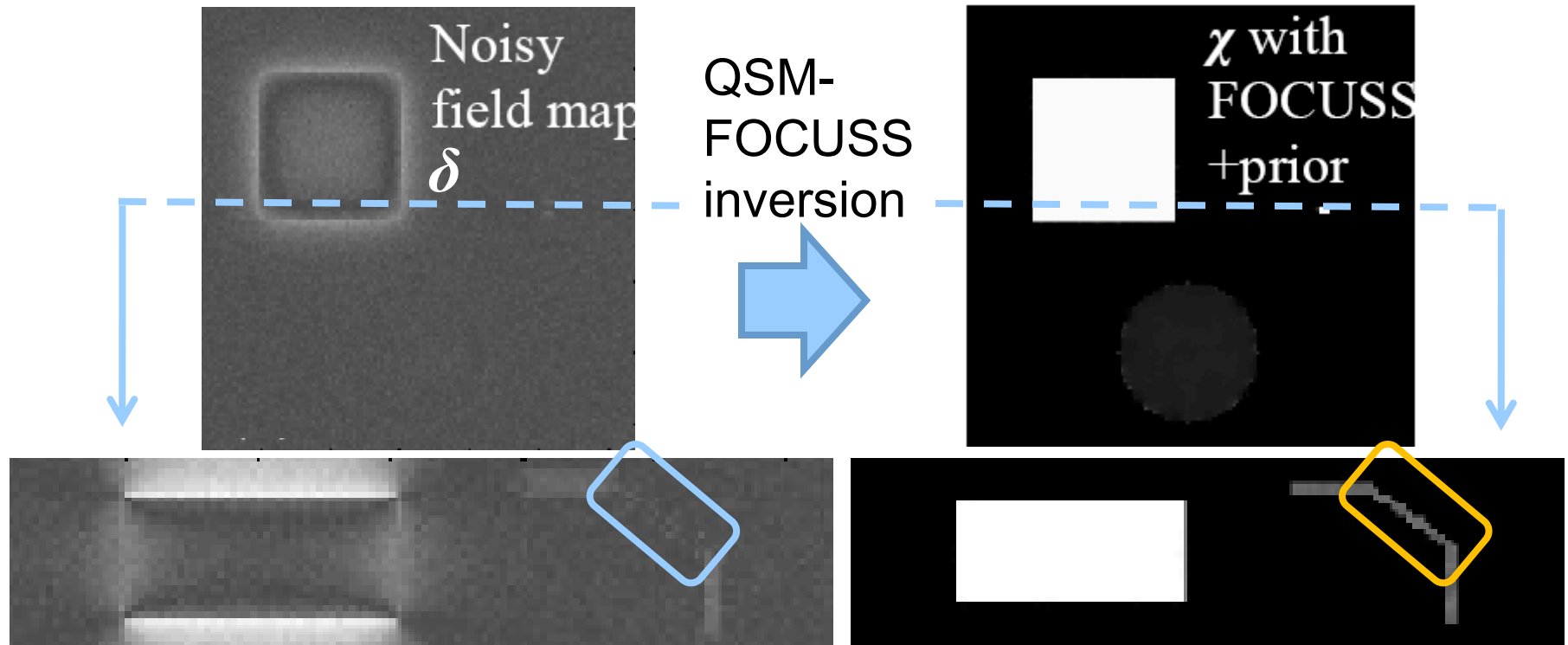
$$\chi = \operatorname{argmin}_{\theta} \underbrace{\sum_{r=x,y,z} \|\partial_r \theta - \partial_r \chi\|_2^2}_{\text{matching gradients}} + \beta \cdot \underbrace{\|\delta - \mathbf{F}^{-1} \mathbf{D} \mathbf{F} \theta\|_2^2}_{\text{data consistency}}$$

QSM result: FOCUSS-QSM with magnitude prior



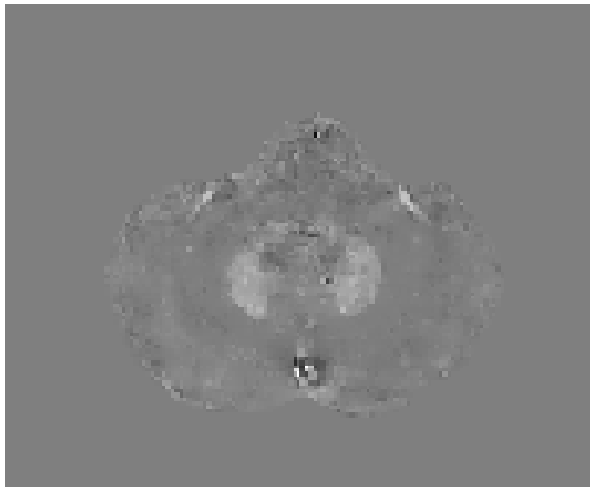
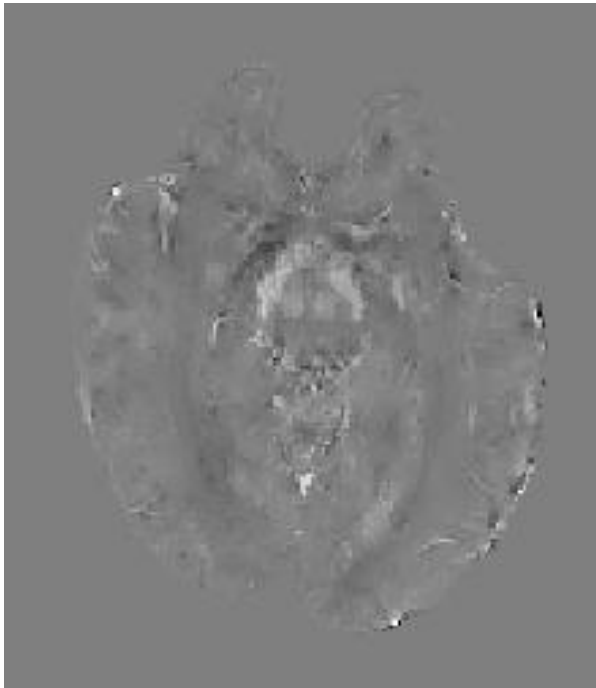
- Starting from the noisy field map δ , FOCUSS-QSM with magnitude prior yielded a susceptibility map with 1.3 % RMSE relative to true χ .

QSM result: FOCUSS-QSM with magnitude prior

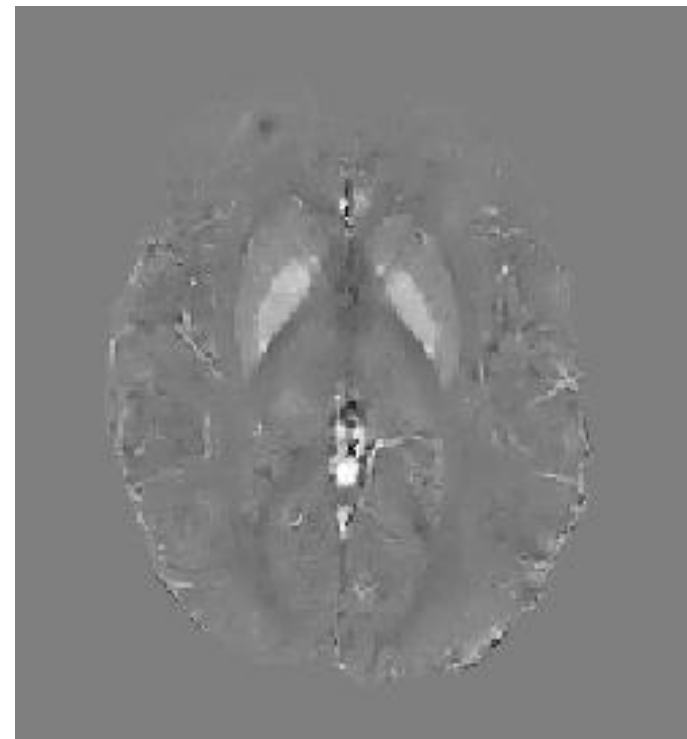


- The reconstructed susceptibility map managed to recover the vessel at the magic angle, which was virtually lost in the field map.

In vivo QSM result: FOCUSS-QSM with magnitude prior

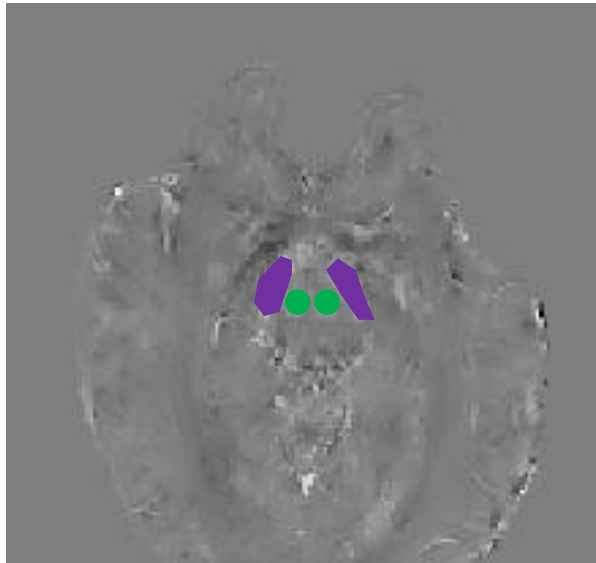


- ❖ 3D GRE acquisition at 3T
- ❖ 32 channel receive array
- ❖ $0.94 \times 0.94 \times 2.5 \text{ mm}^3$ resolution
- ❖ TE: 20 ms



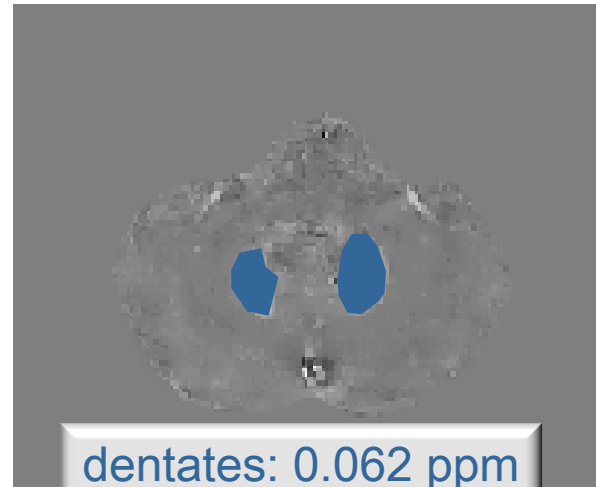
-0.3 ppm  0.3 ppm

In vivo QSM result: FOCUSS-QSM with magnitude prior



subs. nigra: 0.105 ppm

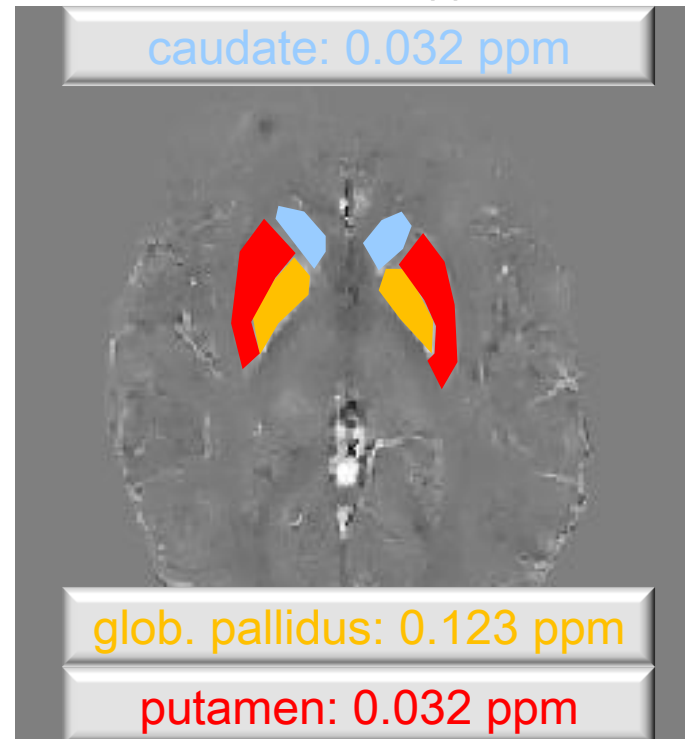
red nuclei: 0.045 ppm



dentates: 0.062 ppm

Structure	$\Delta\chi$ [ppm]
Globus Pallidus	12.3
Substantia Nigra	10.5
Dentate	6.2
Red Nucleus	4.5
Putamen	3.2
Caudate	2.3

x 0.01 ppm, relative to χ_{CSF}



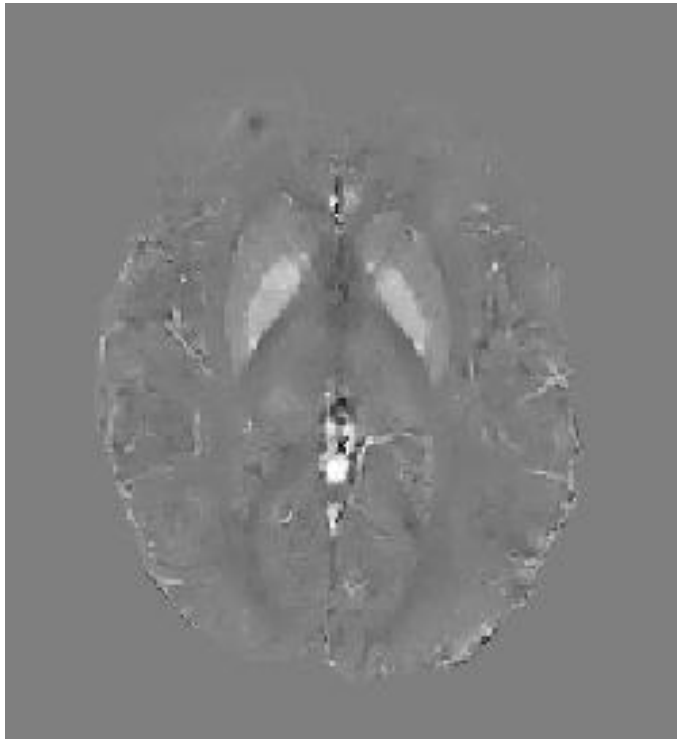
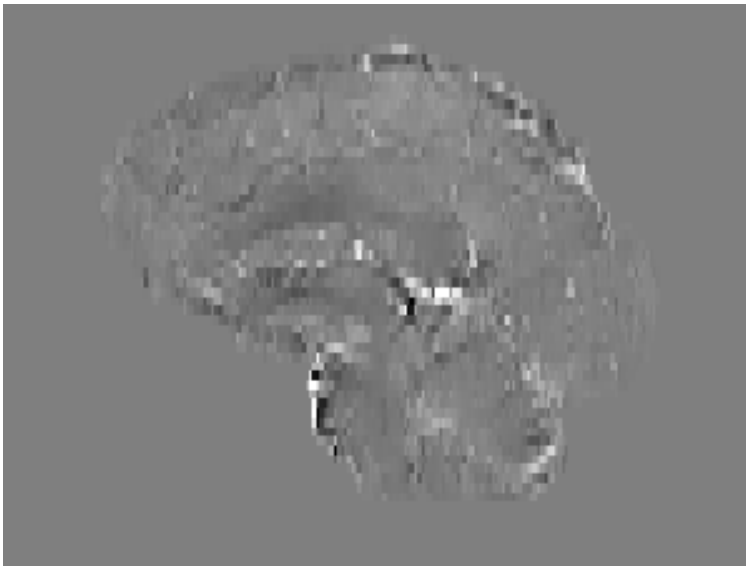
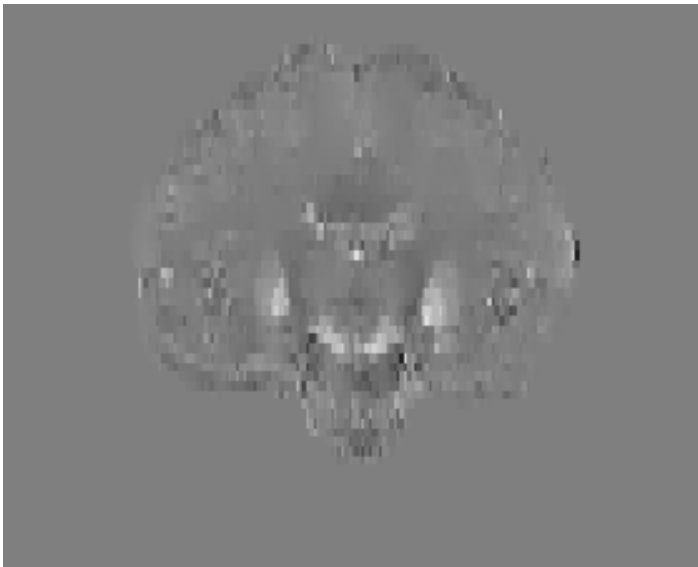
caudate: 0.032 ppm

glob. pallidus: 0.123 ppm

putamen: 0.032 ppm

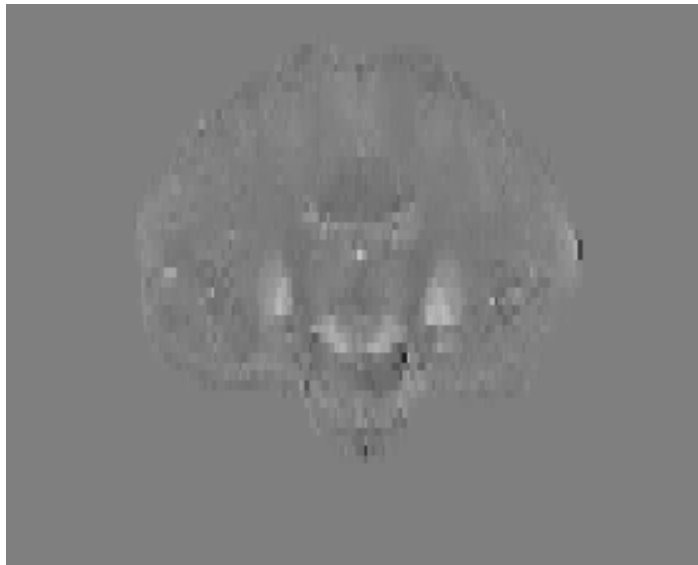
-0.3 ppm 0.3 ppm

In vivo QSM result: FOCUSS-QSM with magnitude prior

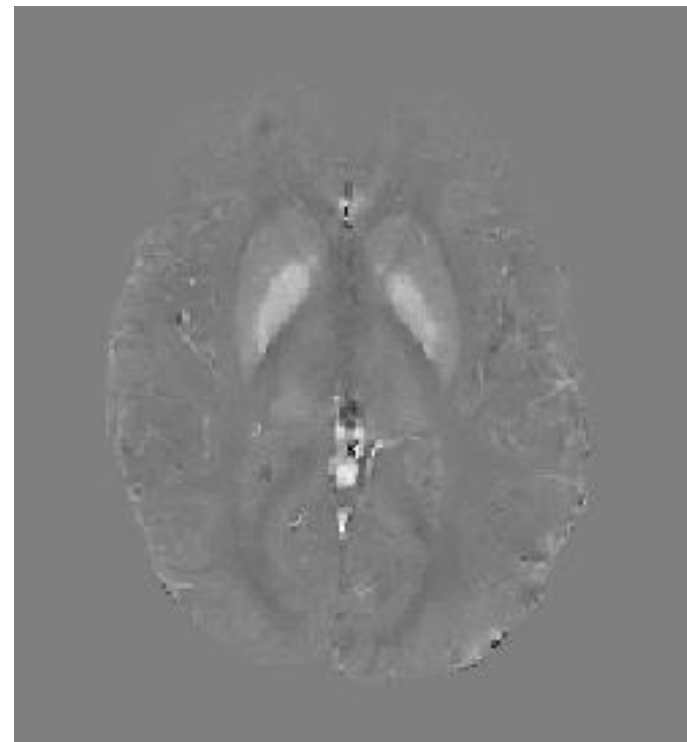
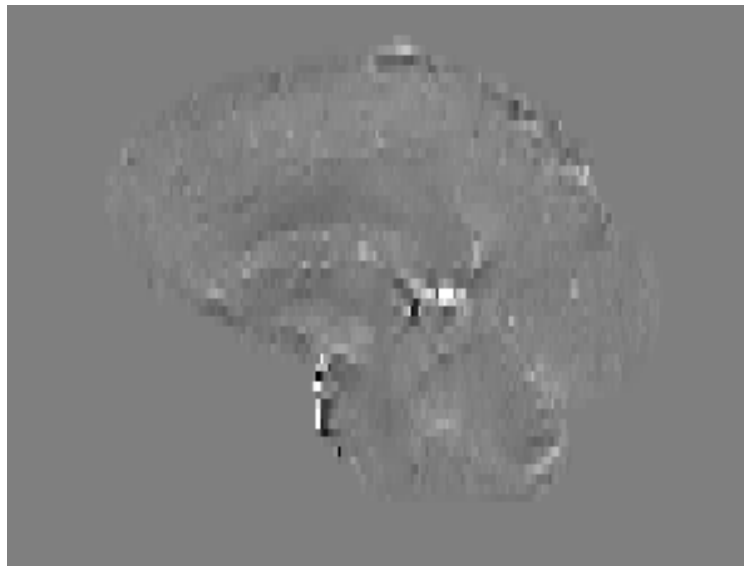


-0.3 ppm  0.3 ppm

In vivo QSM result: FOCUSS-QSM with a prior

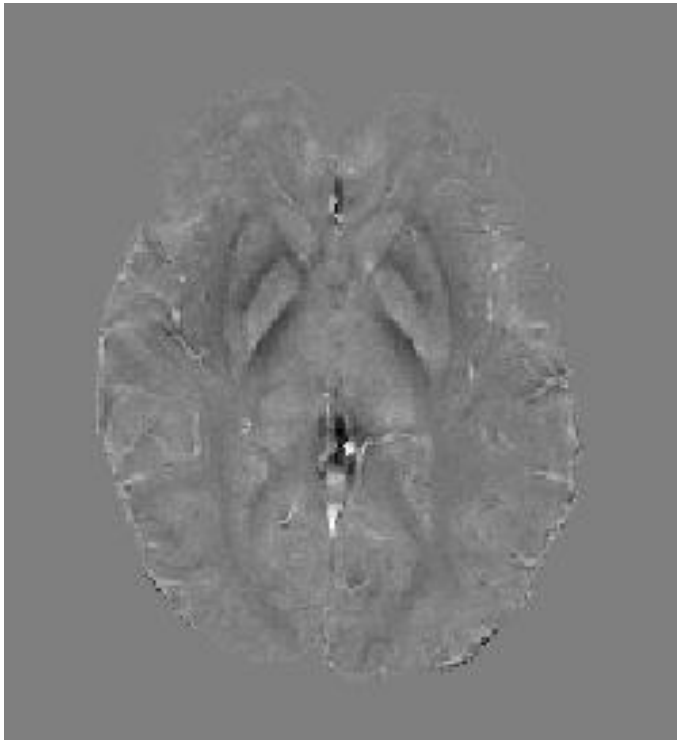
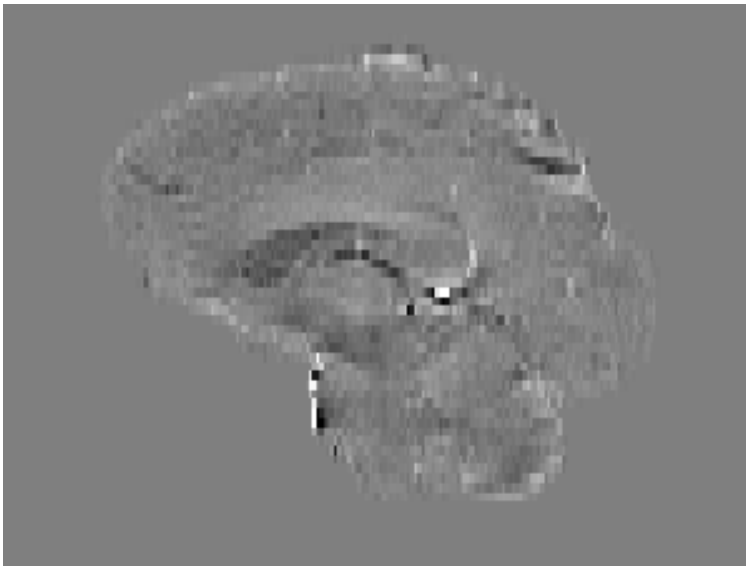
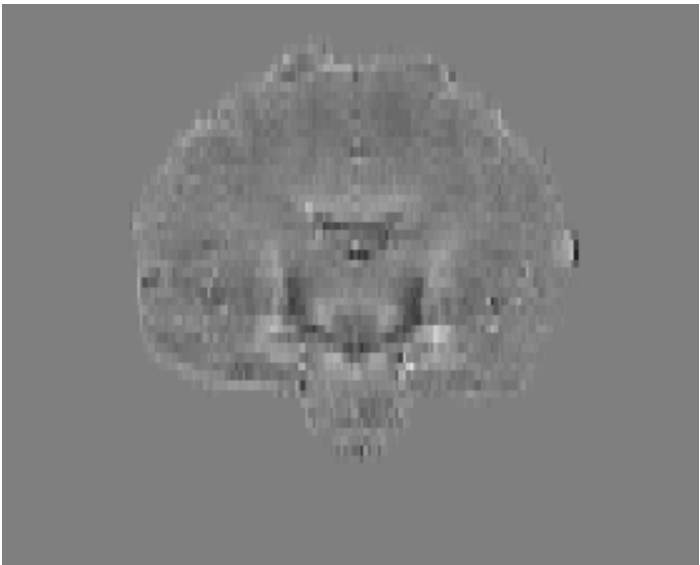


Vessels are less apparent without the magnitude prior



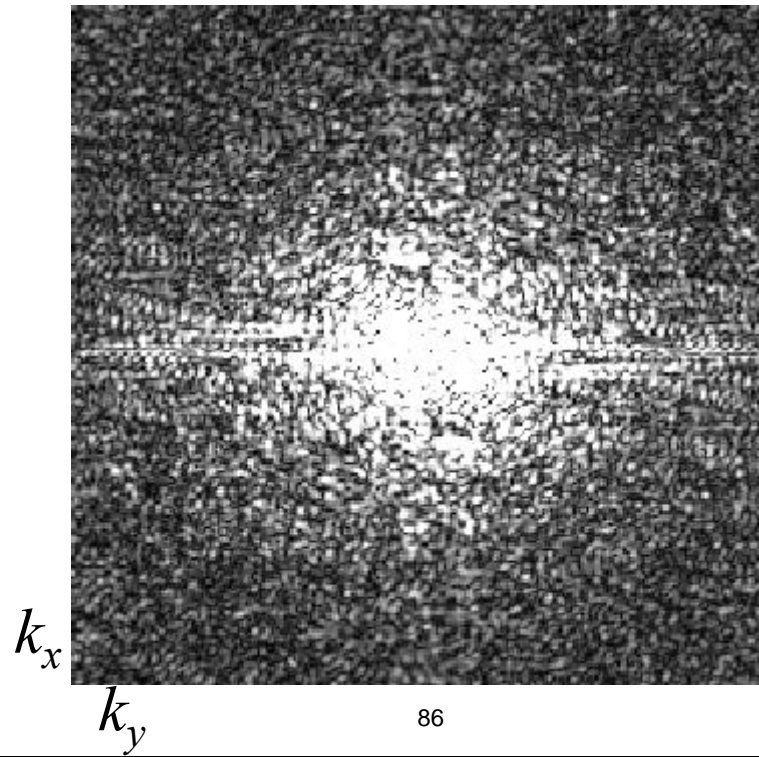
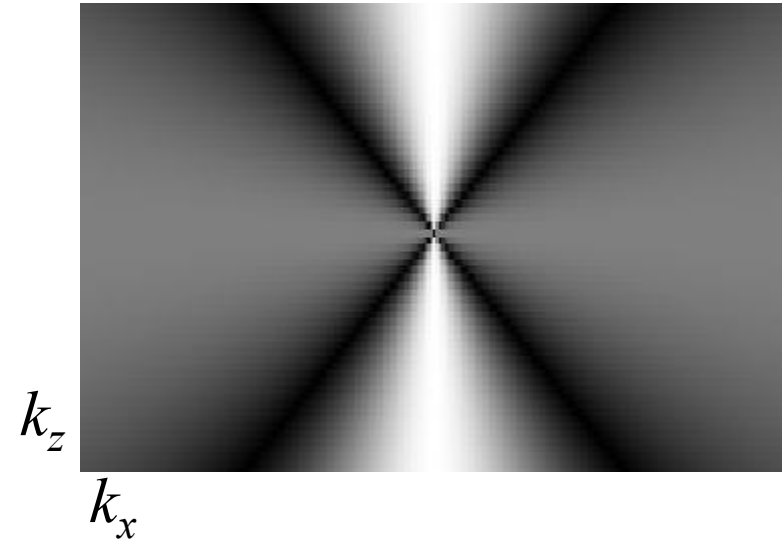
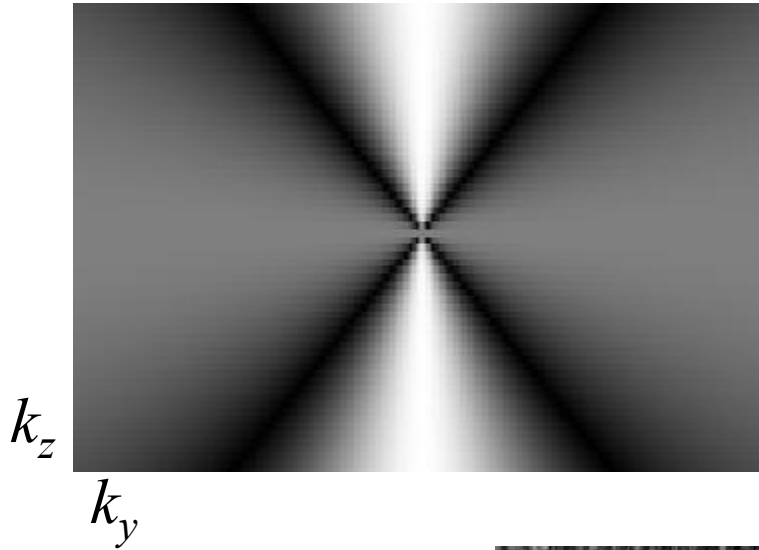
-0.3 ppm  0.3 ppm

Corresponding Tissue Field Map:

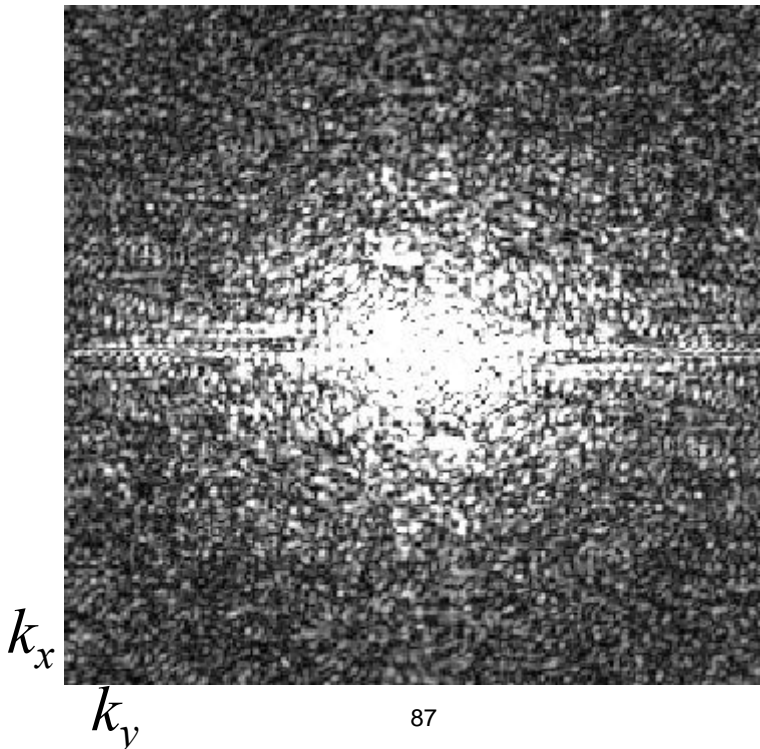
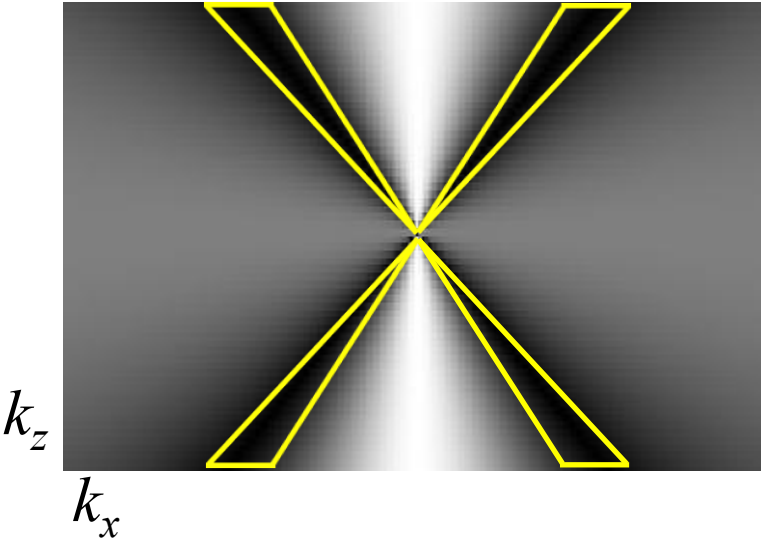
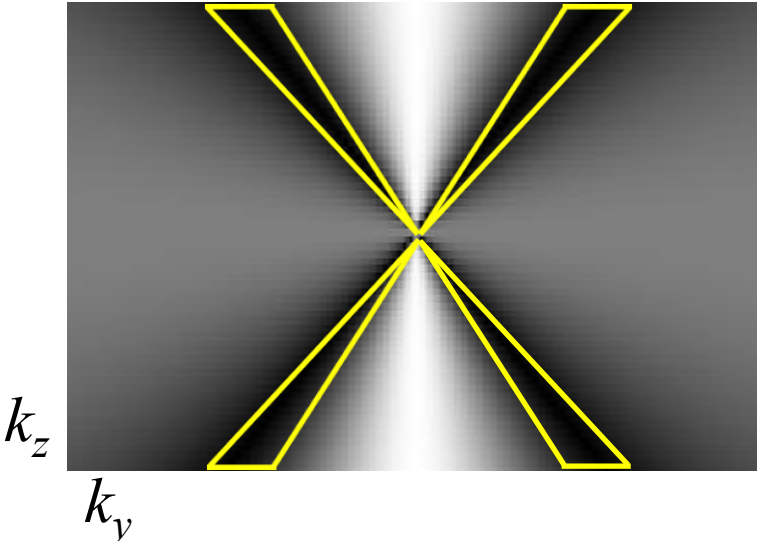


-0.1 ppm  0.1 ppm

In vivo QSM result with magnitude prior in k-space:



In vivo QSM result with magnitude prior in k-space:



Potential drawbacks of FOCUSS-QSM

- Computation time:
 - ❖ Dipole fitting for background removal \approx 2 hours
 - ❖ FOCUSS-QSM \approx 1 hours
 - ❖ Total processing time \approx **3 hours** for data of size [256x256x64]

Potential drawbacks of FOCUSS-QSM

■ Computation time:

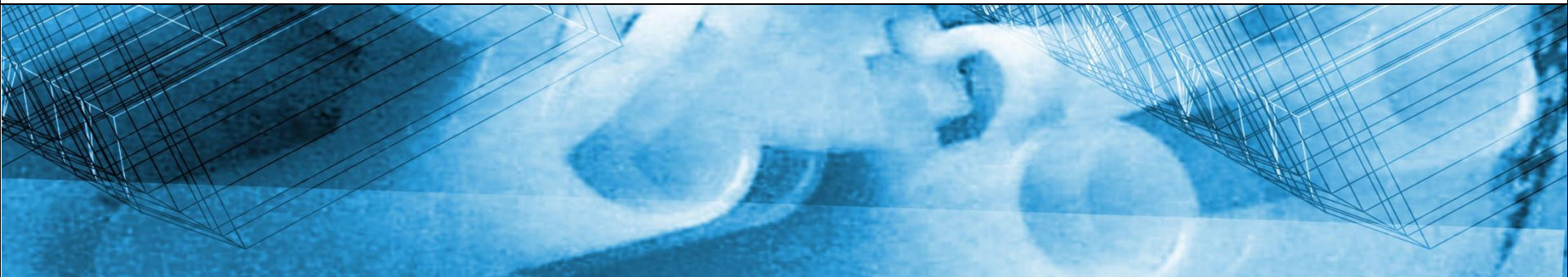
- ❖ Dipole fitting for background removal \approx 2 hours
- ❖ FOCUSS-QSM \approx 1 hours
- ❖ Total processing time \approx **3 hours** for data of size [256x256x64]

■ Solution:

- ❖ Both algorithms solve Least Squares problems, Graphics Processing Card (GPU) implementation will greatly enhance the performance

Conclusion

- Starting with a multi-coil 3D GRE acquisition, we outlined coil combination and background phase elimination methods that yielded the tissue field map.
- We introduced a Quantitative Susceptibility Mapping algorithm that makes use of the magnitude image to facilitate the kernel inversion.



Estimating Brain Iron Concentration in Normal Aging using L1-QSM

Berkin Bilgic¹, Adolf Pfefferbaum^{2,3}, Torsten Rohlfing²,
Edith V. Sullivan³, and Elfar Adalsteinsson^{1,4}

¹ EECS, MIT, Cambridge, MA, United States

² Neuroscience Program, SRI International, USA

³ Department of Psychiatry and Behavioral Sciences, Stanford University School of Medicine, Stanford, CA, USA

⁴ Harvard-MIT Division of Health Sciences and Technology, Cambridge, MA, United States

L1 Regularized Susceptibility Inversion

- Again, we are seeking the susceptibility map that matches the observed tissue phase,

$$\text{Find } \chi \text{ such that } \delta = \mathbf{F}^{-1}\mathbf{DF} \chi$$

- The susceptibility values are tied to the paramagnetic properties of the underlying tissues; hence they vary smoothly across space within anatomical boundaries.
- Based on this, we model the susceptibility map to be approximately piece-wise constant,
- And formulate this belief by invoking sparsity inducing L1 norm on the spatial gradients of χ

L1 Regularized Susceptibility Inversion

- We solve for the susceptibility distribution with a convex program,

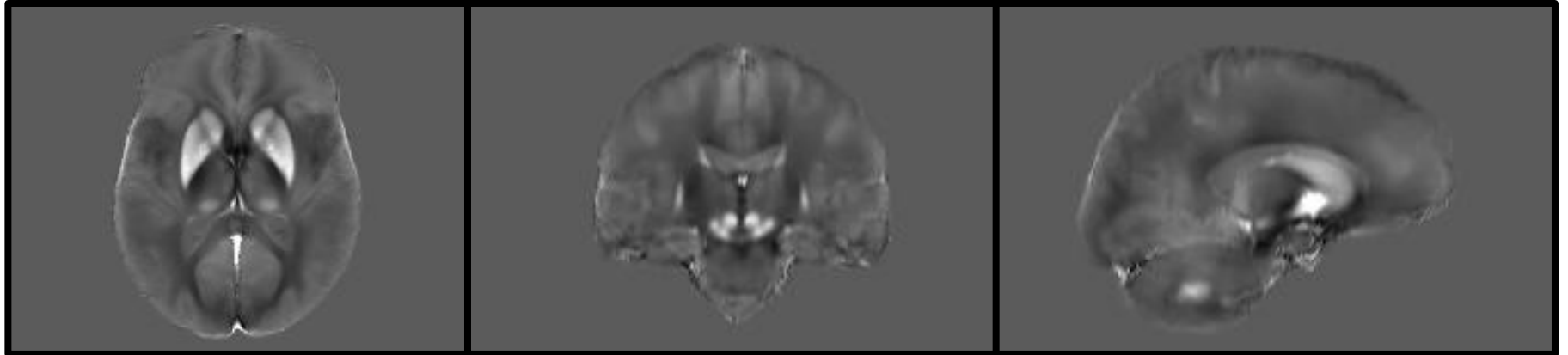
$$\chi_{\text{tissue}} = \operatorname{argmin}_{\chi} \|\delta - \mathbf{F}^{-1} \mathbf{D} \mathbf{F} \chi\|_2^2 + \lambda (\|\partial_x \chi\|_1 + \|\partial_y \chi\|_1 + \|\partial_z \chi\|_1)$$

- We call this method L1-QSM, for which λ serves as a regularization parameter that adjusts the smoothness of the solution
- This is essentially the same formulation as FOCUSS-QSM, but is less sophisticated as magnitude information is not used

Tissue iron deposition in young and elderly subjects

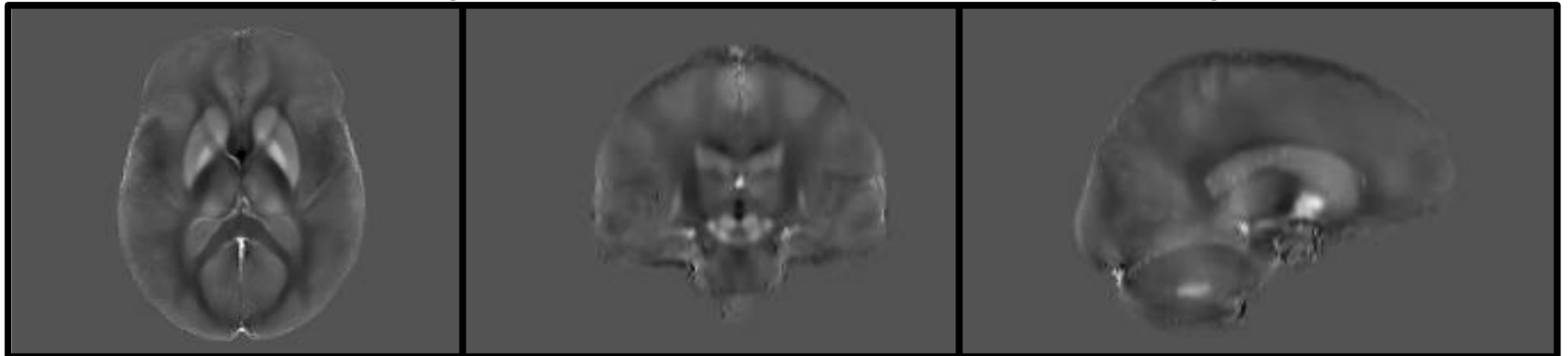
- Tissue susceptibility is a sensitive marker of iron concentration, however it is partially influenced by myelin, proteins etc.
- In this study, we used L1-QSM to test the hypothesis that, **iron deposition in striatal and brain stem nuclei would be greater in older than younger adults**
- Subjects:
11 younger adults (age = 24.0 ± 2.5) and
12 elderly adults (age = 74.4 ± 7.6)
- Data:
Susceptibility Weighted 3D SPGR at 1.5 T

Average L1-QSM Result for the Elderly

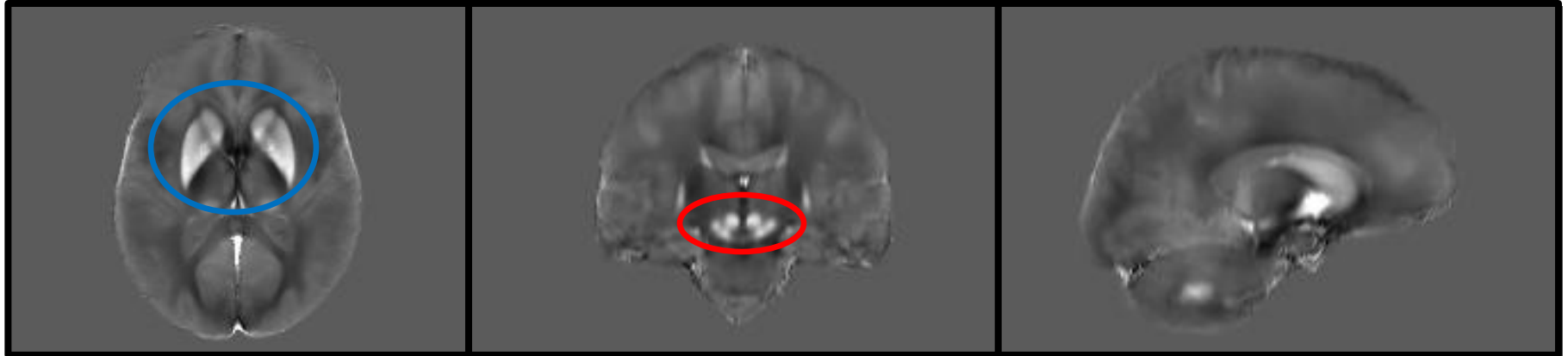


-0.1 ppm 0.16 ppm

Average L1-QSM Result for the Young



Average L1-QSM Result for the Elderly

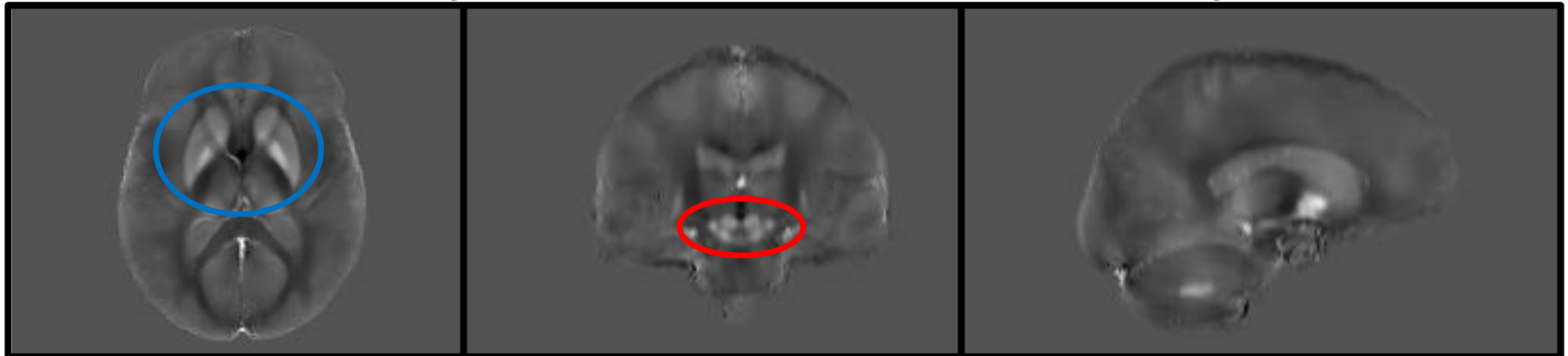


Striatal ROIs

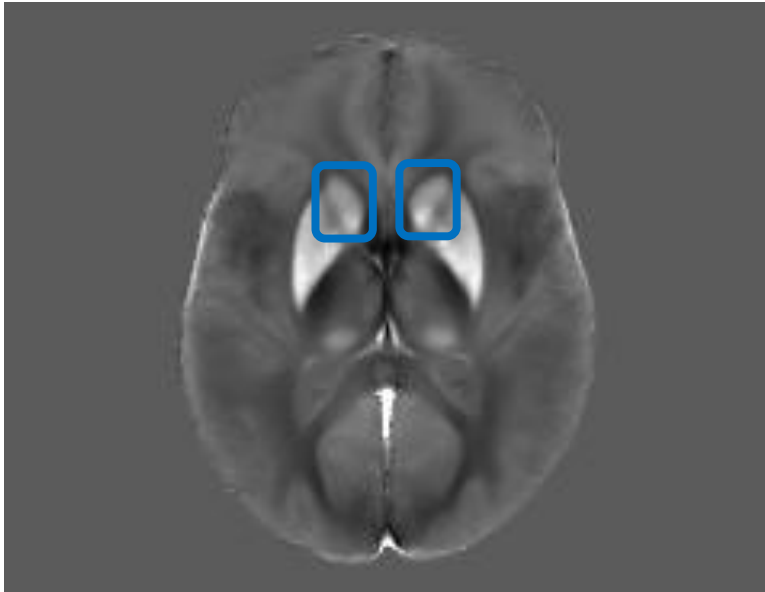
Brain Stem ROIs

-0.1 ppm 0.16 ppm

Average L1-QSM Result for the Young

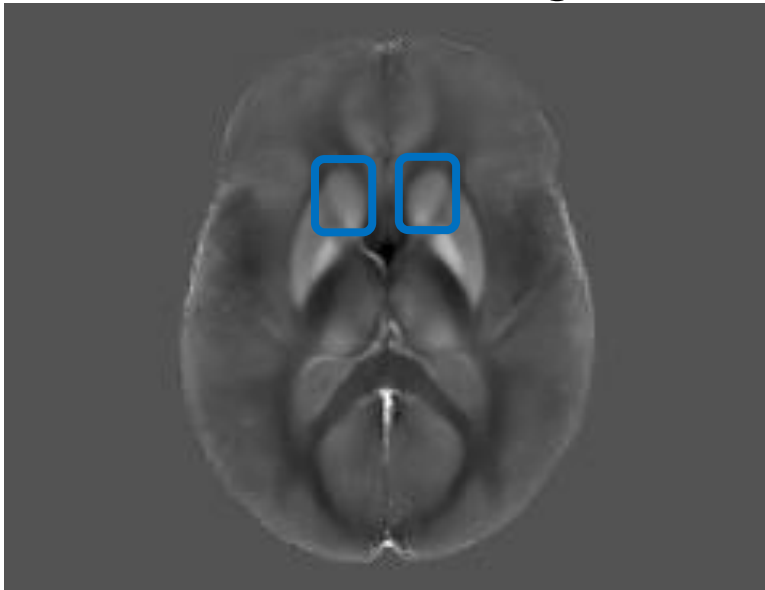


Average L1-QSM Result for the Elderly



Elderly caudate nucleus: 0.059 ppm

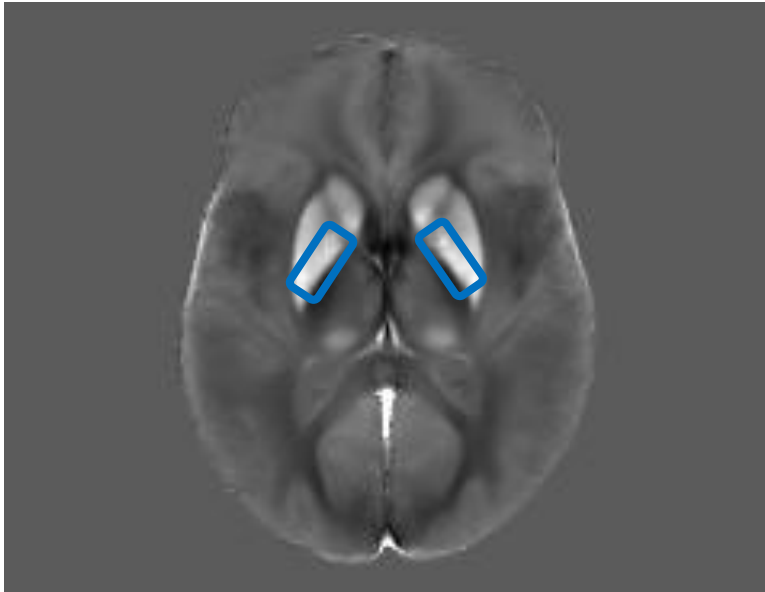
Average L1-QSM Result for the Young



Young caudate nucleus: 0.023 ppm

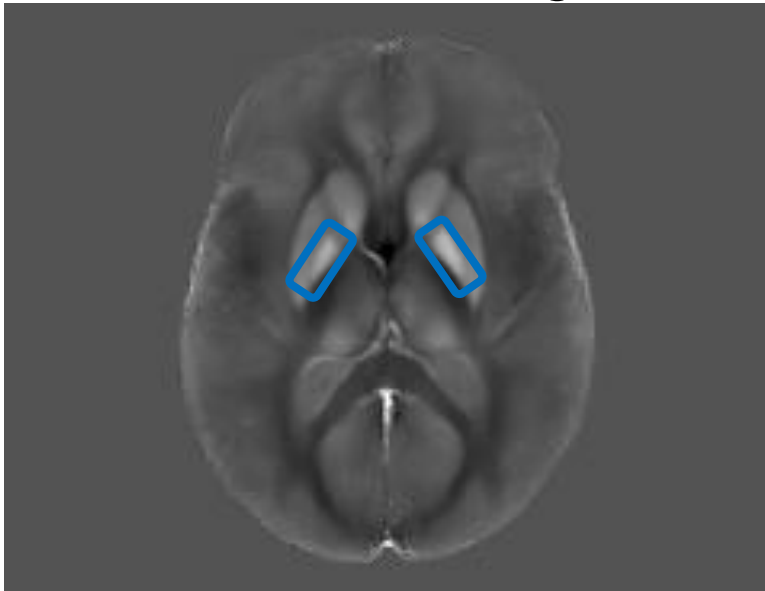
t-test result: **p < 0.0001**
significant

Average L1-QSM Result for the Elderly



Elderly globus pallidus: 0.120 ppm

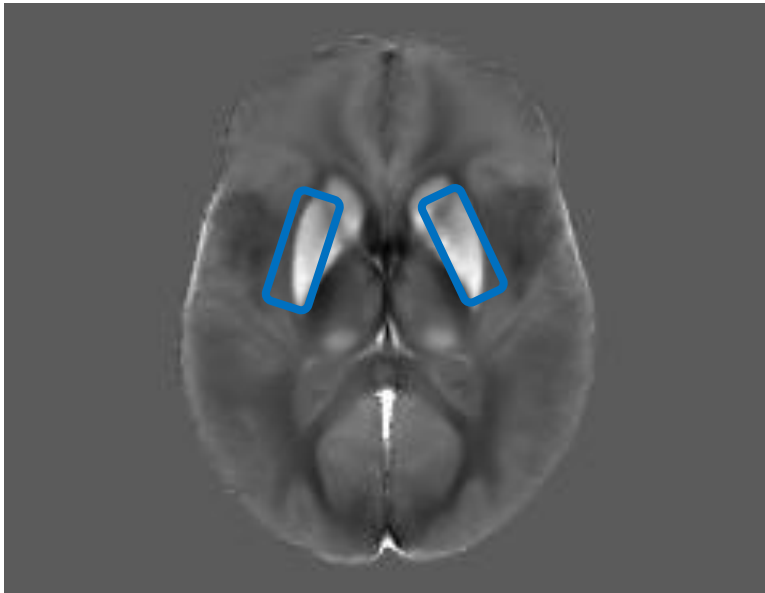
Average L1-QSM Result for the Young



Young globus pallidus: 0.069 ppm

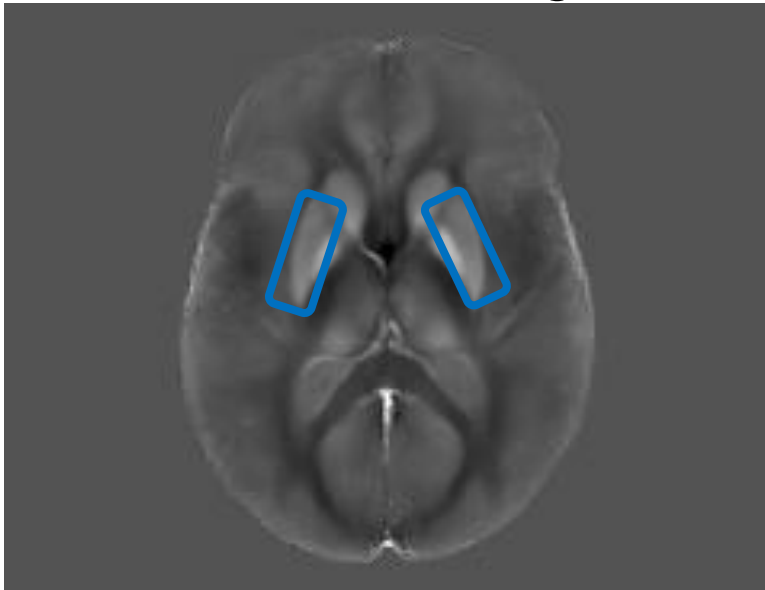
t-test result: **p < 0.0001**
significant

Average L1-QSM Result for the Elderly



Elderly putamen: 0.095 ppm

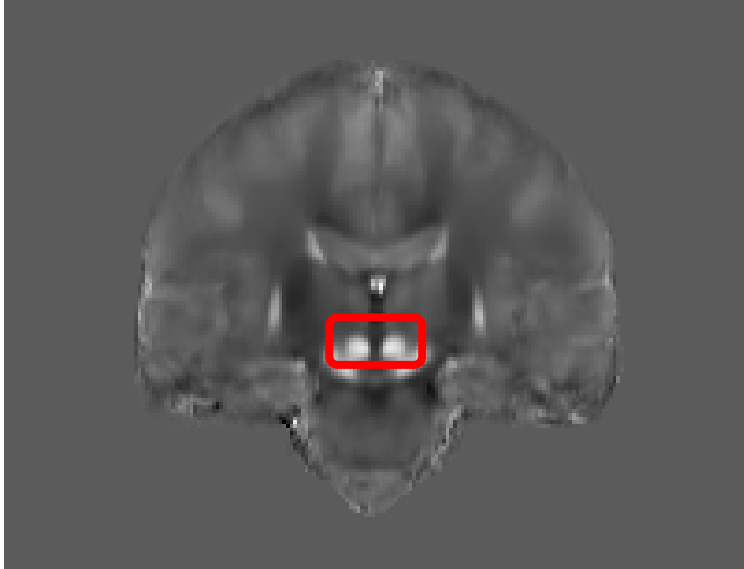
Average L1-QSM Result for the Young



Young putamen: 0.024 ppm

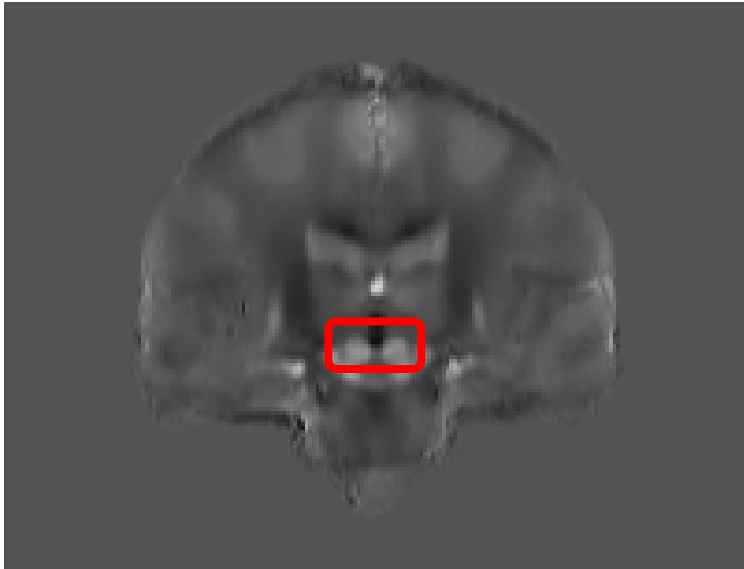
t-test result: **p < 0.0001**
significant

Average L1-QSM Result for the Elderly



Elderly red nucleus: 0.091 ppm

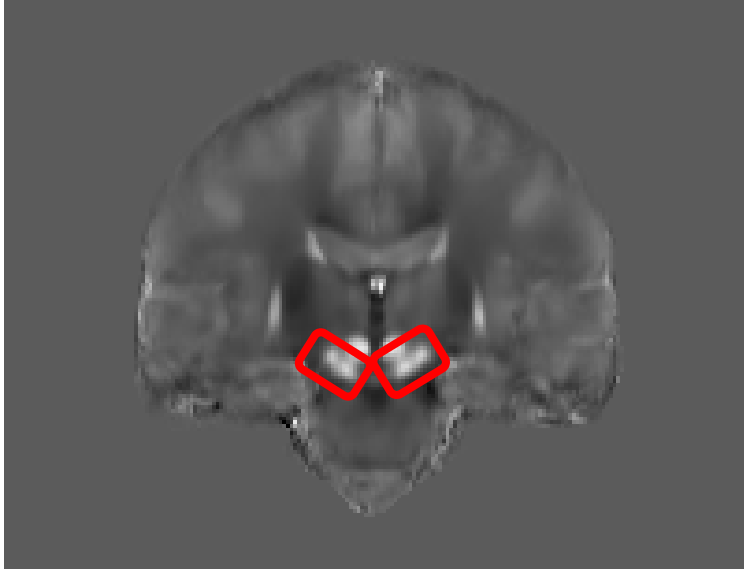
Average L1-QSM Result for the Young



Young red nucleus: 0.030 ppm

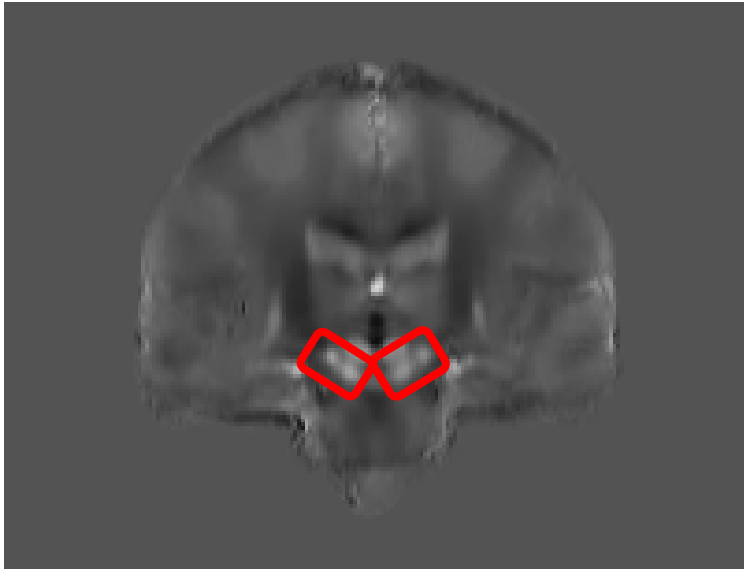
t-test result: **p = 0.0008**
significant

Average L1-QSM Result for the Elderly



Elderly substantia nigra: 0.055 ppm

Average L1-QSM Result for the Young

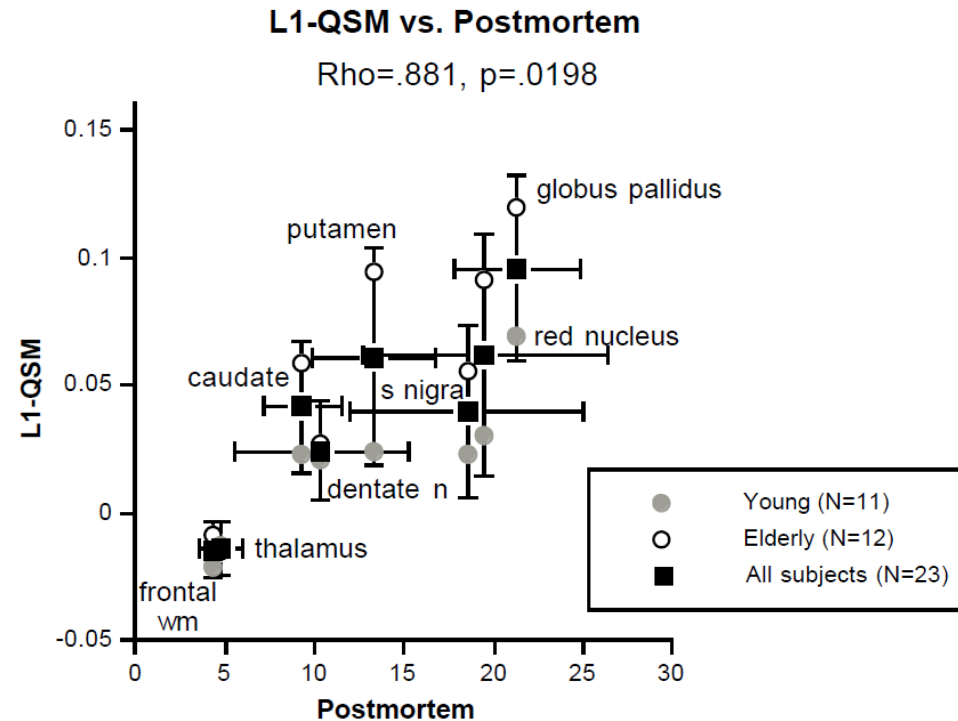


Young substantia nigra: 0.023 ppm

t-test result: **p = 0.0178**
significant

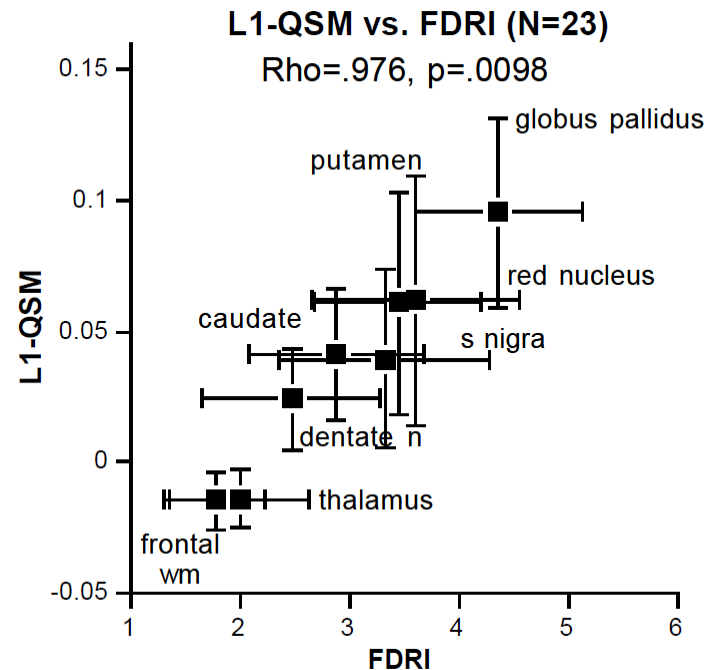
L1-QSM vs. Postmortem

- L1-QSM results correlate well with published postmortem results¹, with $Rho = 0.881$, $p = 0.0198$



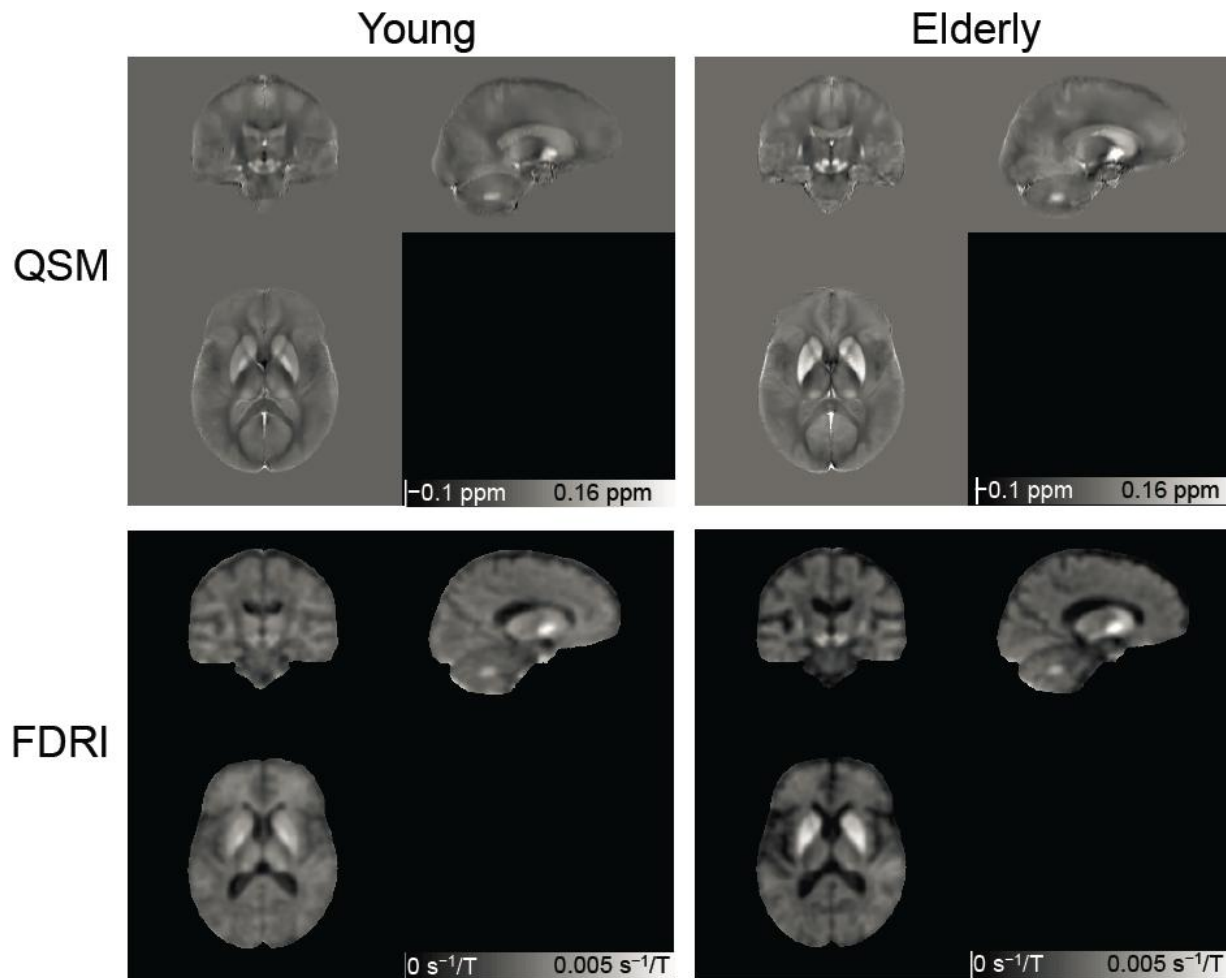
L1-QSM vs. FDRI

- Field-Dependent Relaxation Rate Increase (FDRI)¹ is another iron quantification that requires data acquisition at two different main field strengths.
- L1-QSM is strongly correlated with FDRI results, with $Rho = 0.976$, $p = 0.0098$



L1-QSM vs. FDRI

- L1-QSM requires data acquisition at a single main magnetic field strength, and has much higher spatial resolution, enabling iron quantification in vessels.



Effect of regularization parameter λ

